Using IR Thermography to Evaluate Temperature Distributions on a Diesel NO_X Adsorber Catalyst during Simulated Operation

by

Khurram Aftab

A thesis
presented to the University of Waterloo
in fulfillment of the
thesis requirement for the degree of

Master of Applied Science
in
Chemical Engineering

Waterloo, Ontario, Canada, 2007

AUTHOR'S DECLARATION

I hereby declare that I am the sole author of this thesis. This is a true copy of the thesis, including any required final revisions, as accepted by my examiners.

I understand that my thesis may be made electronically available to the public.

Khurram Aftab

Abstract

In emissions catalyst applications, an axial distribution of reaction, surface chemistry, and temperature all exist on or along the surface of the catalyst. Understanding these distributions is very important in developing physically relevant models of such systems. One focus of this work was developing a technique to obtain accurate temperature measurements from a catalyst during exothermic or endothermic reaction steps. IR thermography was tested as a method to evaluate spatial temperature distributions as a function of time on a diesel NO_X adsorber catalyst. The technique proved accurate, relatively simple to interpret and operate, and efficient to the extent it can be used for data generation.

As a continuation of the technique development, the temperature changes and gradients formed during simulated operation of a $Pt/Ba/Al_2O_3$ NO_X adsorber catalyst (NAC) for diesel exhaust applications were monitored using IR thermography and standard thermocouples. NACs operate in a cyclic manner; during the lean phase, when the engine is in normal operation, the catalyst traps entering NO_X; once the catalyst nears saturation, the catalyst is exposed to a rich exhaust phase, in reductant relative to oxygen, where the trapped NO_X is reduced to N_2; and finally the exhaust returns to the normally lean conditions thereby completing the cycle. During the rich phase, previous work has suggested that significant temperature changes might be occurring along the length of the catalyst. In this study, temporally and spatially resolved temperature distributions were obtained throughout the cycle in order to evaluate the significance of these temperature changes and their effects on the reaction chemistry. The effects of (1) reactor in the possible reaction pathways, (2) CO and O_2 levels in the regeneration phase, (3) NO and NO_2 as the source of NO_X in the lean cycle and (4) nominal operating temperature on these temperature distributions were evaluated. The temperature gradient and distribution measurements are being used to characterize the reactions and as input into models.

Acknowledgements

All praise to Almighty God (Allah) who is the only source of knowledge and without whose mercy coming this far would only have remained a dream.

I would like to express my profound and sincere appreciation to my Supervisor Professor William Epling for his patronage, unflinching support, valuable advice & able guidance, constant encouragement and most of all his kindness.

I would like to highlight my gratitude to Professor William A. Anderson & Professor Robert Hudgins for their constructive feed back and for the hours they put in reviewing this thesis.

My special thanks to Professor Ali Elkamel for his kindness and encouragement throughout my study period.

Worth mentioning is the help, cooperation and encouragement received from all my friends and co-researchers especially in the Reaction Eng & Catalysis Research group. Thank you folks for some great conversations we had over the past years, you all made my stay very cordial.

I would like to thank Department of Chemical Engineering for the opportunity and the necessary facilities to carry out this research especially Pat, Rick & Dennis who were always around to help out

I acknowledge NSERC and Cummins Inc for providing financial assistance for this project.

Lastly my gratitude goes to my family for teaching me the value of education, hard work, patience, sacrifice, and honesty. They have been a source of great encouragement and moral support through these years even if they weren't quite sure what I was doing.

Dedication

To my mother Professor Dr. Shahnaz Aftab who provided me with endless encouragement and support. And to my father late Aftab Shahid (your memories live on) I dedicate this thesis.

Table of Contents

List of Figures

List of Tables

Chapter 1: Introduction

1.1 Origin of Air Pollutants

Air pollutants are substances that adversely affect the environment by interfering with factors such as climate, plant physiology, and ecosystems. Global climate change is one of the most important environmental challenges facing mankind in the 21st century. Air pollutants can originate from natural or man-made sources, or both. Some examples of natural sources include volcanic eruptions or wind erosion, and man-made sources include combustion engines.

The industrialization of the world has been accompanied by a drastic increase in the consumption of fossil and synthetic fuels. The fuel energy is freed mostly by means of combustion processes that also result in emission of pollutants, many from incomplete combustion. Subsequent reactions can also transform primary pollutants into different chemical species, which can in some cases be more harmful than their precursors. Some of the most important air pollutants, their sources, and known or suspected environmental effects are listed in Table 1-1.

1.2 Legislation

Governments and international organizations are establishing guidelines and laws to protect the quality of air, and to control emissions of climate changing agents. For example, in the United States America, the Environmental Protection Agency (EPA) is required to set National Ambient Air Quality Standards (NAAQS) under the Clean Air Act of 1990 for wide-spread pollutants from various sources which are considered harmful to public health and the environment.

The NAAQS set two types of air quality standards.

1) Primary standards (human health) - The purpose is to protect sensitive members of the human population (asthmatics, children, and the elderly) from any adverse health effects of air pollutants.

Table 1-1: Some air pollutants and a highlight of their sources and effects [49, 50]

Pollutant	Natural Source	Man made Source	Environmental Effect
Nitrogen oxides	Lightning, soil bacteria	High temperature fuel combustion—motor vehicles, industrial, and utility	Photochemical smog, destruction of stratospheric ozone, acid rain, human health impact.
Particulates	Forest fires, wind erosion, volcanic eruption	Combustion of biofuels such as wood, and fossil fuels such as coal or diesel	Reduced atmospheric visibility, human health impact, contribution to global warming.
Sulfur dioxide	Volcanic eruptions and biological decay	Coal combustion, ore smelters, petroleum refineries, diesel engines high-sulfur fuels	Acid rain, human health impact.
Carbon monoxide	Wild fires	Rich & stoichiometric combustion, mainly from motor vehicles	Human health impact
Carbon dioxide	Animal respiration, biological decay	Fossil fuel and wood combustion	Common greenhouse gas
(VOC)	Biological processes	Incomplete combustion, solvent utilization	Photochemical smog

2) Secondary standards (public welfare) - To protect public welfare from any adverse effects due to the presence of the pollutant in the air. Public welfare effects include effects on soils, water, crops, vegetation, man made materials, animals, wildlife, weather, visibility, climate, and damage to and deterioration of property etc.

Various pollutant limits set by different environmental agencies are listed in Table 1-2. The particular limits are averages over different periods of time.

Table 1-2: Selected ambient air quality standards by some agencies [50, 51, 52]

Pollutant	Av. time	US (NAAQS)	California	WHO
Ozone	1 hr	0.12 ppm	0.09 ppm	-
	8 hr	0.08 ppm	0.07 ppm	120 $\mu g/m^3$
Carbon Monoxide	1 hr	35 ppm	20 ppm	30,000 $\mu g/m^3$
	8 hr	9.4 ppm	9 ppm	10,000 $\mu g/m^3$
PM_{10}	24 hr	150 $\mu g/m^3$	50 $\mu g/m^3$	-
$PM_{2.5}$	24 hr	35 $\mu g/m^3$	-	-
Nitrogen Dioxide	1 hr	-	0.250 ppm	200 $\mu g/m^3$
	1 yr	0.053ppm	-	40 $\mu g/m^3$
Sulfur Oxides	24 hr	0.14 ppm	-	125 $\mu g/m^3$
	1 yr	0.03 ppm	-	50 $\mu g/m^3$

1.3 What is NO_X?

This section is focused on one of the major air pollutants, NO_X, some of its adverse effects and major sources of NO_X emissions. Nitrogen oxide (NO_X) is a general term and can be used to refer to any of the oxides of nitrogen, or to a mixture of them, including nitric oxide (NO), nitrogen dioxide (NO_2), nitrous oxide (N_2O), and dinitrogen trioxide (N_2O_3). Nitrogen oxides can form when fuel is burned at high temperatures, as in a combustion process. The visible colored gaseous product amongst them is nitrogen dioxide (NO_2), which is reddish-brown in color and sometimes appears over many urban areas. In atmospheric chemistry the term NO_X is used to mean the total concentration of NO plus NO_2 and this definition will be used in this thesis.

1.4 Why Remove NO_X?

NOx causes major health and environmental concerns. Some of the adverse effects are listed below [50].

1) Ground-Level Ozone (Smog) is formed when NO_X and volatile organic compounds (VOCs) react in the presence of heat and sunlight. Causing damage to lung tissue, vegetation and reducing crop yields, NO_2 is one of the main ingredients involved in the formation of ground-level ozone, which can trigger serious respiratory problems.

2) Visibility Impairment can result when nitrate particles and nitrogen dioxide block the transmission of light, reducing visibility in urban areas and on a regional scale.

3) Water Quality Deterioration can occur with increased nitrogen loading in water bodies, upsetting the chemical balance of nutrients used by aquatic plants and animals. Additional nitrogen accelerates "eutrophication" which leads to oxygen depletion and reduces fish and shellfish populations. For example, NO_X emissions in the air are one of the largest sources of nitrogen pollution in the Chesapeake Bay [50].

4) Acid Rain can form from NO_X reacting with other substances in the air to form acids which fall to earth as rain. Acid rain deteriorates vegetation, damages cars, buildings and historical monuments; and causes lakes and streams to become acidic and unsuitable for many fish.

5) Global Warming originates from a variety of natural and man-made sources. Nitrous oxide is considered a strong greenhouse gas causing global warming. It accumulates in the atmosphere with other greenhouse gases causing a gradual rise in the earth's temperature. This leads to increased risks to human health, a rise in the sea level, and other adverse changes to plant and animal habitats.

6) Toxic Chemicals can be produced in the air since NO_X reacts readily with organic chemicals and ozone, some of which may cause biological mutations. Examples of these compounds include nitrate radicals, nitroarenes, and nitrosamines [50].

Figure 1-1 provides a summary regarding the sequence of negative events caused by the introduction of NO_X into the environment by any human activities.

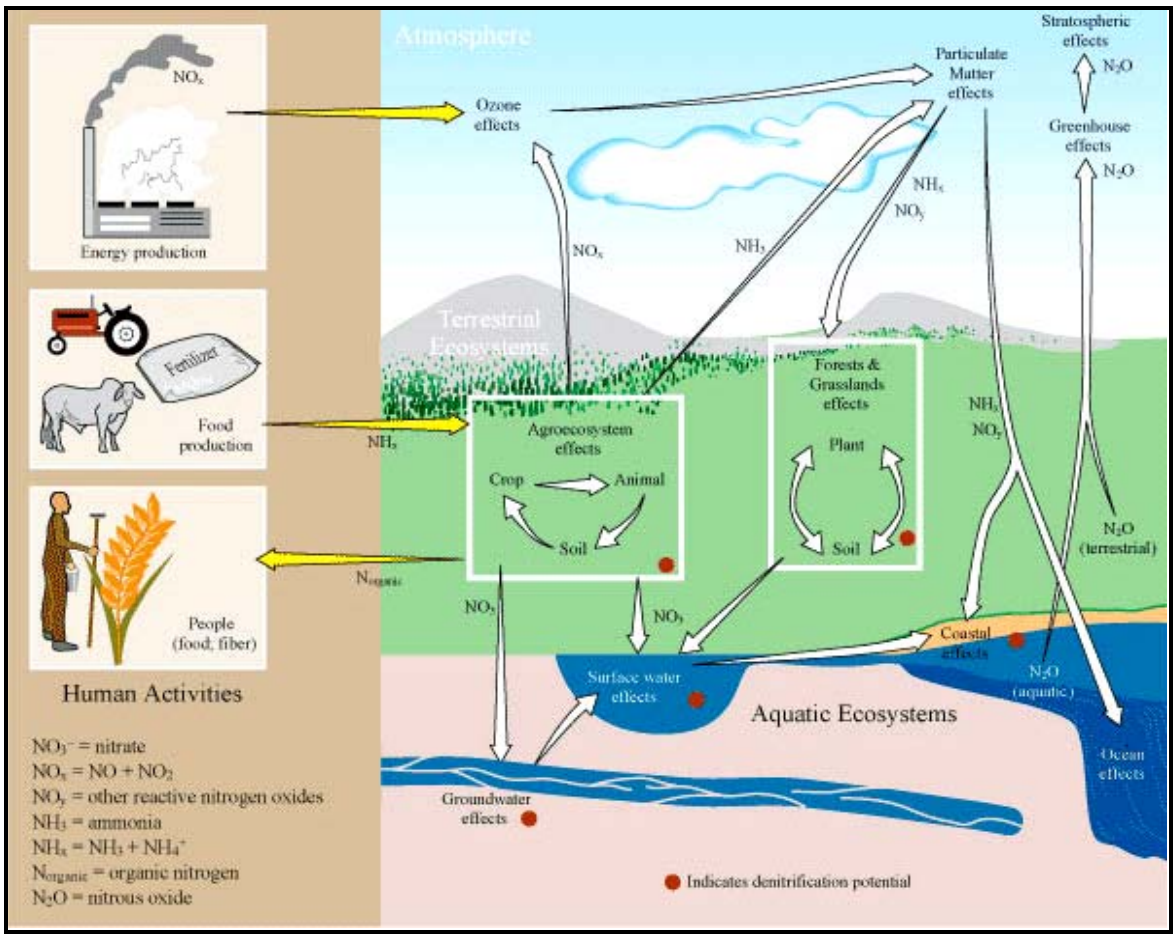

Figure 1-1: Environmental NO_X cycle taken from the UNEP website [53]

1.5 Sources of NO_X

Man-made sources of NO_X are far greater in comparison to that from natural processes; see Figure 1-2. As shown, it is clear that the major source of NO_X emissions are transportation and electric utilities, both of which make use of fossil fuel combustion.

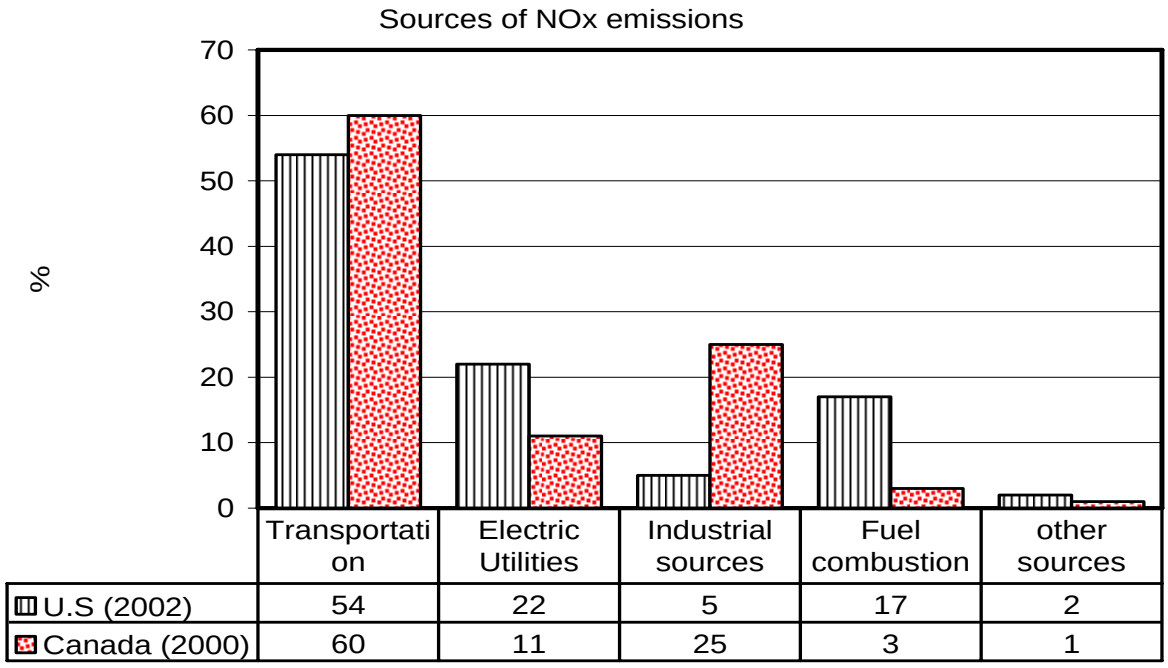

Figure 1-2: NO_X emissions for various sources in Canada & U.S [54]

1.5.1 Internal Combustion Engine

In an internal combustion engine, an exothermic reaction between a fuel and an oxidizer occurs in a confined space called a combustion chamber. When the temperature exceeds 1700 K during combustion, the constituents of air start to react, resulting in various nitrogen oxide compounds. The combustion reaction along with the NO formation reaction is:

$C_mH_n + (m+n/4)O_2 \rightarrow mCO_2 + (n/2)H_2O$ (combustion reaction)

$N_2 + O_2 \rightarrow 2NO$ (NO formation reaction)

The resultant gases from the combustion reaction (Fig 1-3) then expand to provide power. These engines appear in a wide variety of automobiles, locomotives, jets, and large ships, the

latter usually in the form of turbines where very high power was required. Another application of combustion is electric power generation by industries.

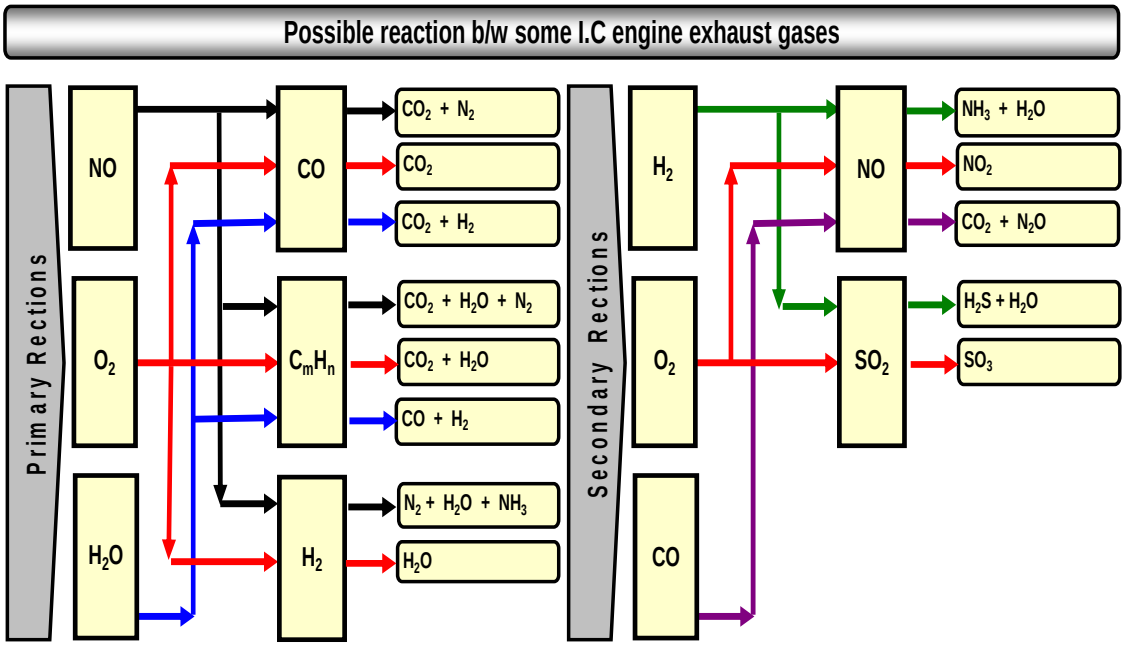

Figure 1-3: Common reaction between gases in the exhaust of an internal combustion engine

1.5.1.1 Lean Burn Engine

The internal combustion engine operating on a lean air to fuel mixture ratio is called a lean burn engine.

Air to fuel ratio (A / F) = mass of air consumed / mass of fuel consumed

The term lean mixture is applied to gasoline engines when the stoichiometric air to fuel ratio is higher than 14.7. To maintain this A/F ratio in an engine results in increase fuel consumption. An air/fuel at the stoichometric ratio i.e 14.7 will result in near optimum fuel mileage, costing less per mile traveled and producing the least amount of emissions. On the other hand the draw back of burning lean is the large amount of NO_X generated which then requires something other than a 3-way catalyst converter which does not work in these conditions. Diesel engines have a high air to fuel ratio and are an example of a lean burn

engine. Emissions of carbon monoxide and hydrocarbons from diesel engines are significantly lower than those from gasoline engines as they burn the fuel in excess air. Similarly diesel NO_X emissions are usually lower than those from gasoline engines but higher than those from gasoline engines equipped with a three-way catalyst. Figure 1-4 shows some differences between the diesel engine and gasoline engine.

A drawback of the diesel engine is its high particulate matter mass emissions that are practically absent from gasoline exhaust gases. Emissions of particulate matter and NO_X are the focus of today's diesel emission control technologies and our study will focus on NO_X emissions from a diesel engine.

Diesel Engines		Petrol Engines	
Pros	**Cons**	**Pros**	**Cons**
Lower fuel costs	Maintenance is more expensive	Light - hence more portable	Not so durable
Higher efficiencies	Heavier and bulkier for a given power	Lower capital costs	Long-term usage
Readily available for a wide range of sizes and applications	Higher capital cost	Cheaper to maintain	Lower efficiency for equivalent power
Lower running speeds	Pollution	Higher running speeds	Fuel more expensive / Pollution

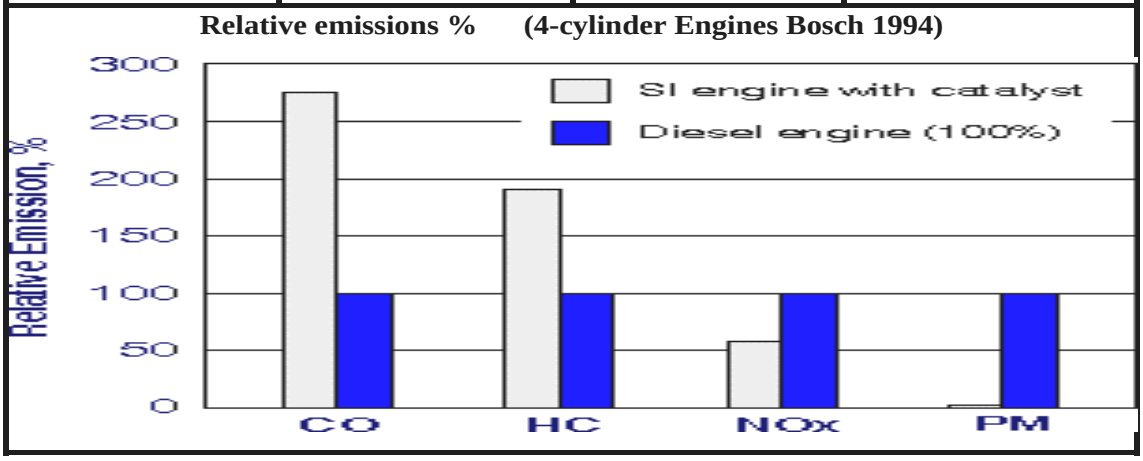

Figure 1-4: Some common comparisons between diesel and petrol engines [48]

1.6 Diesel Engines

A diesel engine is a compression ignition engine, in which the fuel is injected during the compression stroke and it ignites due to high heat and pressure in the engine. This is different from gasoline engine where the fuel is mixed first and then ignited by a spark plug. So there is a short time for fuel to react with all the oxygen in the cylinder of the diesel engine compared to a gasoline engine, where air and fuel are mixed for the entire compression stroke.

1.6.1 Principle

Diesel fuel combustion works on the principle that during gas compression, the temperature increases, and will result in ignition of the fuel. Air taken in the cylinder of a diesel engine is compressed by the moving piston at a much higher compression ratio than used in a gasoline engine. At the end of the piston stroke, diesel fuel is injected into the combustion chamber at the high pressure through an atomizing nozzle.

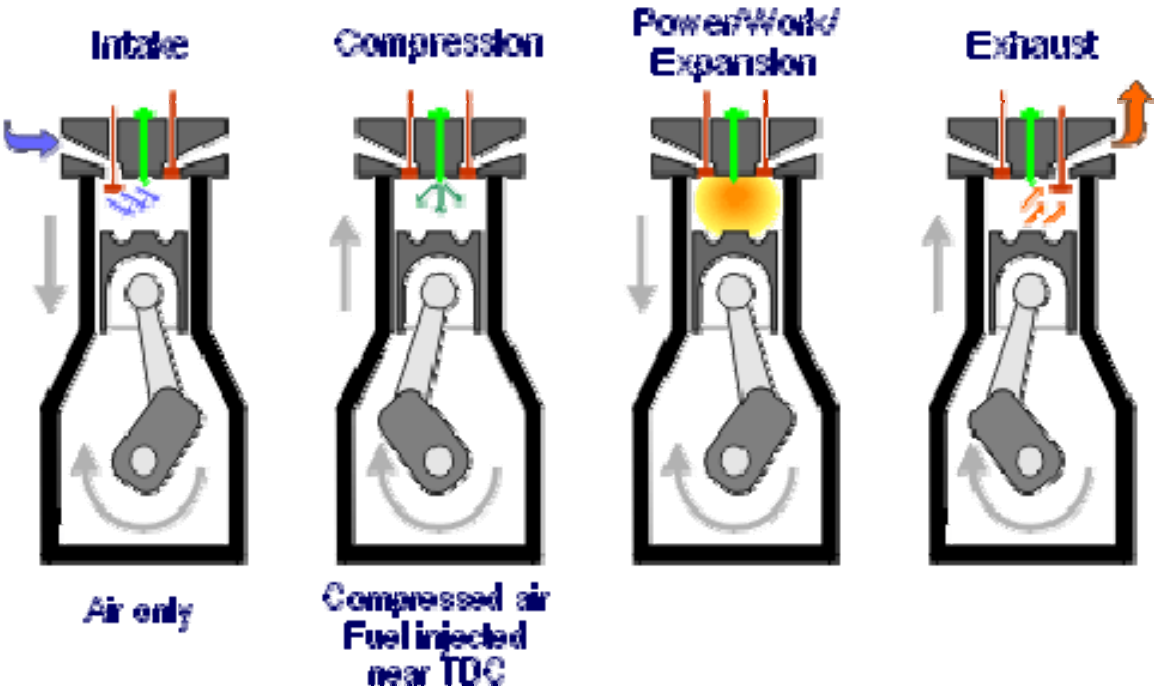

Figure 1-5: 4-stroke diesel engine operation [48]

The fuel ignites as soon as it comes in contact with the hot air. The combustion causes the gas in the chamber to further heat up and increases its pressure, Figure 1-5, which in turn forces the piston outward and finally moves the crankshaft. Diesel engines are more efficient than gasoline engines of the same power, resulting in lower fuel consumption. A common margin is 40% more fuel efficient (miles per gallon) than the gasoline engine [49].

1.6.2 Diesel Engine Applications

The vast majority of heavy road vehicle trucks, ships, many buses, many commercial boats, heavy tractors, military vehicles, a few passenger cars, a few large vans and SUV's, large-scale portable power generators, most farm and mining vehicles, and many long-distance locomotives use diesel engines.

1.6.3 Diesel Engine Exhaust

Diesel engine exhaust consists of a mixture of combustion reactants and products. The emissions from a car engine can be described as:

1) Primary Emissions:

- Nitrogen gas (N_2) - Air is 78% nitrogen gas, and most of this passes right through the engine.
- Carbon dioxide (CO_2) - This is one product of combustion. The carbon in the fuel bonds with the oxygen in the air.
- Water vapor (H_2O) - This is another product of combustion. The hydrogen in the fuel bonds with the oxygen in the air.

2) Secondary Emissions:

As the combustion process is never perfect, other products and some reactants are also exhausted and include:

- Carbon monoxide (CO) – Is a colorless and odorless poisonous gas which is produced from incomplete combustion of C with O_2.
- Volatile organic compounds (VOCs) – These are organic chemical compounds that under normal conditions have high enough vapor pressures to significantly vaporize

and enter the atmosphere. These are carbon based compounds, and form from incomplete combustion of fuel with oxygen.

- Nitrogen oxides / dioxides (NO_X) – NO_X is a major contributor towards the formation of smog, acid rain and results in adverse effects as described earlier.

With the passage of time, emissions having adverse effects towards humans and the environment are raising more and more concern. In order to deal with these emissions, a lot of work is being carried out by the government, private and public sectors.

1.7 Emission Control in Engine Exhaust

A major source of nitrogen oxides is burning fuel at high temperatures, as in combustion processes, and the most common combustion process today occurs in the engines of automobiles. Over time, two control strategies aimed at curtailing the engine emissions for environmental regulations have evolved.

1. First Phase

Initial progress in controlling engine emissions, primarily starting in the 1980's, was achieved by adapting engine technologies to reduce target species. At that time exhaust after treatment was unable to compete with the engine modification technologies due to catalyst deactivation as the result of use of lead in the fuels. For engine technologies, some of the developments include:

a) Modifications in the fuel injection system
b) Changes in the combustion chamber design
c) Improved methods for air intake for combustion
d) Improved fuel/air ratios for optimized fuel combustion
e) Improved fuel quality (eliminated lead addition to fuels)
f) Exhaust gas recirculation (EGR)
g) In cylinder ceramic (zirconium) coatings to control emissions

With all of these modifications in engine design and other technology applications, there was a 10-fold decrease in emissions over the period from the late 80's to early 2000 [48].

2. Second Phase

The elimination of lead in fuels and the development of new precious metal based after treatment catalysts played a key role for switching the attention from engine technologies towards application of after-treatment methods in order to control emissions. Even with such improvements, to meet emission standards being implemented in the 2005-2010 timeframe, additional emissions reductions technologies will be required, and some of those are described in Table 1-3. Some of the after treatment methods being studied, developed and used include:

a) Three way catalyst,
b) Selective catalytic reduction (SCR) technology,
c) Lean NO_X traps.

Table 1-3: Summary of the 3 catalyst technologies along with the reaction types [48]

Catalyst Technology	Reaction Type	Reduced Emissions
Three way catalyst	Oxidation, Reduction	CO, HC, Particulate matter, NO_X
Selective Catalytic Reduction (SCR)	Selective catalytic reduction by ammonia/urea	NO_X
Lean NO_X Trap (LNT)	Adsorption of NO_X under lean / reduction under rich conditions	NO_X, CO, HC

1.7.1 Catalyst Technologies

The following is a brief description of these catalyst technologies.

1.7.1.1 Three Way Catalytic Converter

This catalyst takes its name from controlling the three major emissions in an engine that are NO_X, VOCs and carbon monoxide. The catalyst commonly contains an alumina wash coat supported on a honeycomb shape ceramic brick as shown in Figure 1-6. Precious metals are coated onto the alumina. The active part of the catalyst is further divided into oxidation and the reduction catalyst sites. The platinum/rhodium components act as the active sites to carry out reduction reactions, while platinum/palladium acts as the active component for oxidation reactions.

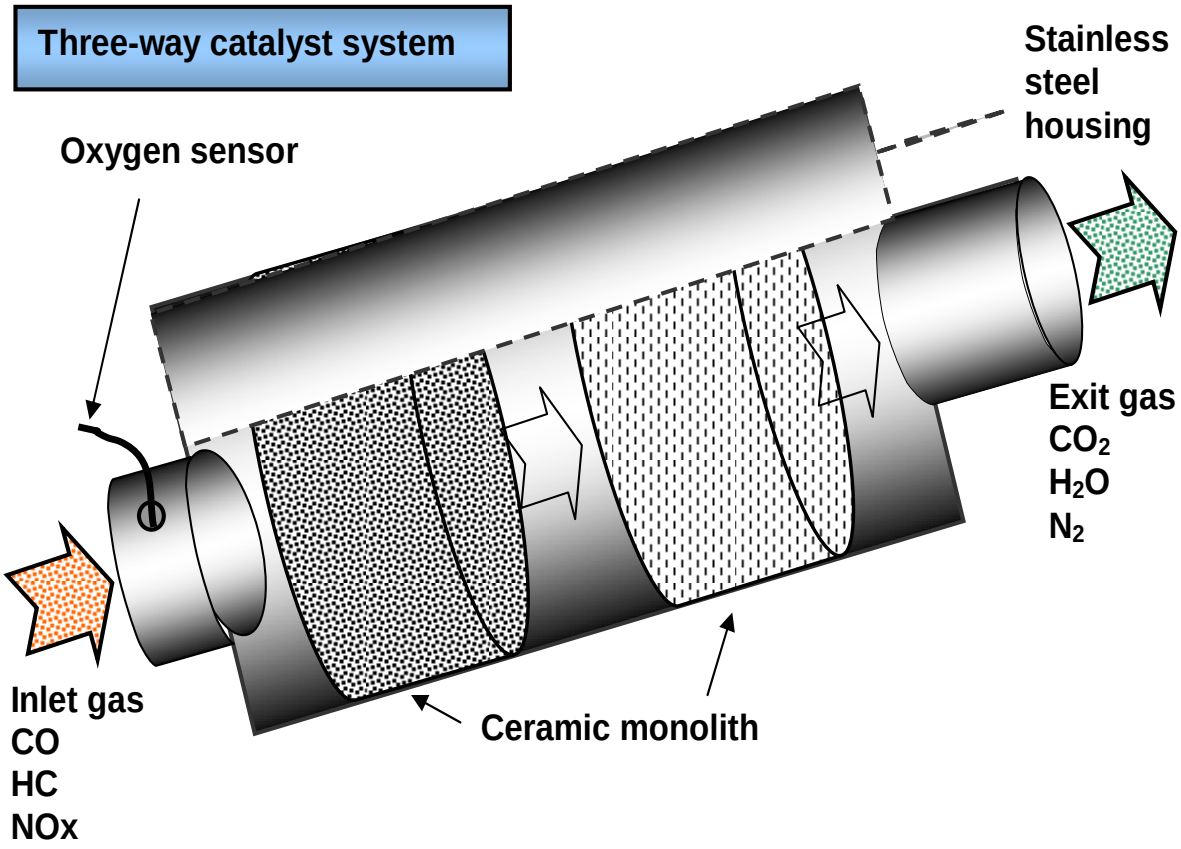

Figure 1-6: Three way catalytic converter inside metal housing

The first stage of the catalytic converter is the **reduction catalyst**. The primary component, in terms of activity, of this part is platinum and rhodium, which help to reduce NO_X emissions. The NO or NO_2 molecule on contact with the catalyst separates the nitrogen atom out of the NO_X molecule. The N_2 and O_2 forms and desorbs.

The reactions are shown below:

$2NO \Rightarrow N_2 + O_2$ or

$2NO_2 \Rightarrow N_2 + 2O_2$

Note, excess oxygen will decrease the conversion of this reaction.

The second stage of the catalytic converter is the **oxidation catalyst**. This part of the catalyst helps to reduce CO and unburned hydrocarbon emissions by oxidation with the help of the remaining oxygen in the exhaust (also the oxygen liberated from the reduction catalyst). The oxidation reaction is carried out in the presence of the platinum and palladium part of the catalyst. The reaction is given as below:

$2CO + O_2 \Rightarrow 2CO_2$

In addition to just the catalyst, there is a control system that monitors and controls the exhaust stream by making changes in the fuel injection system according to best performance requirements in terms of least emissions. The oxygen sensor mounted upstream of the catalytic converter tells the engine the amount of oxygen in the exhaust. So the engine computer can adjust the mixture (air/fuel) to give the engine the best fuel economy with less exhaust emissions. As the three-way catalyst is for rich-burn or stoichiometric engines, closed loop air-fuel ratio controllers are required for it to work effectively. Overall, the combination of the catalyst and control system significantly reduces the emissions from stoichiometric-burn gasoline engines.

1.7.1.2 Selective Catalytic Reduction (SCR)

In SCR technology a reduced nitrogen compound, typically ammonia, or urea as an ammonia precursor, is introduced into the exhaust. The "oxidized" NO, NO_2 or both, then reacts with the ammonia forming elemental nitrogen and water. The reaction is shown below:

Ammonia Reaction

$4NH_3 + NO + O_2 \Rightarrow 4N_2 + H_2O,$ or

$4NH_3 + 2NO_2 + O_2 => 3N_2 + 6H_2O$

Urea Decomposition Reaction

$4(NH_2)\ 2CO => 2NH_3 + CO_2$

The catalyst used is a vanadium-based catalyst, or an Fe- or Cu-based zeolite. Zeolites offer improved durability at high temperatures while vanadium is used for low temperature or high sulfur fuel applications e.g stationary powerplants, diesel-powered ships etc.The catalyst structure consists of a honeycomb ceramic block similar to the 3-way catalyst. The price ranges of these catalysts are much lower than the technologies that require platinum.

One drawback is the requirement for either an ammonia or urea vessel in the automobile body, Figure1-7. Such systems are commercially available for stationary applications.

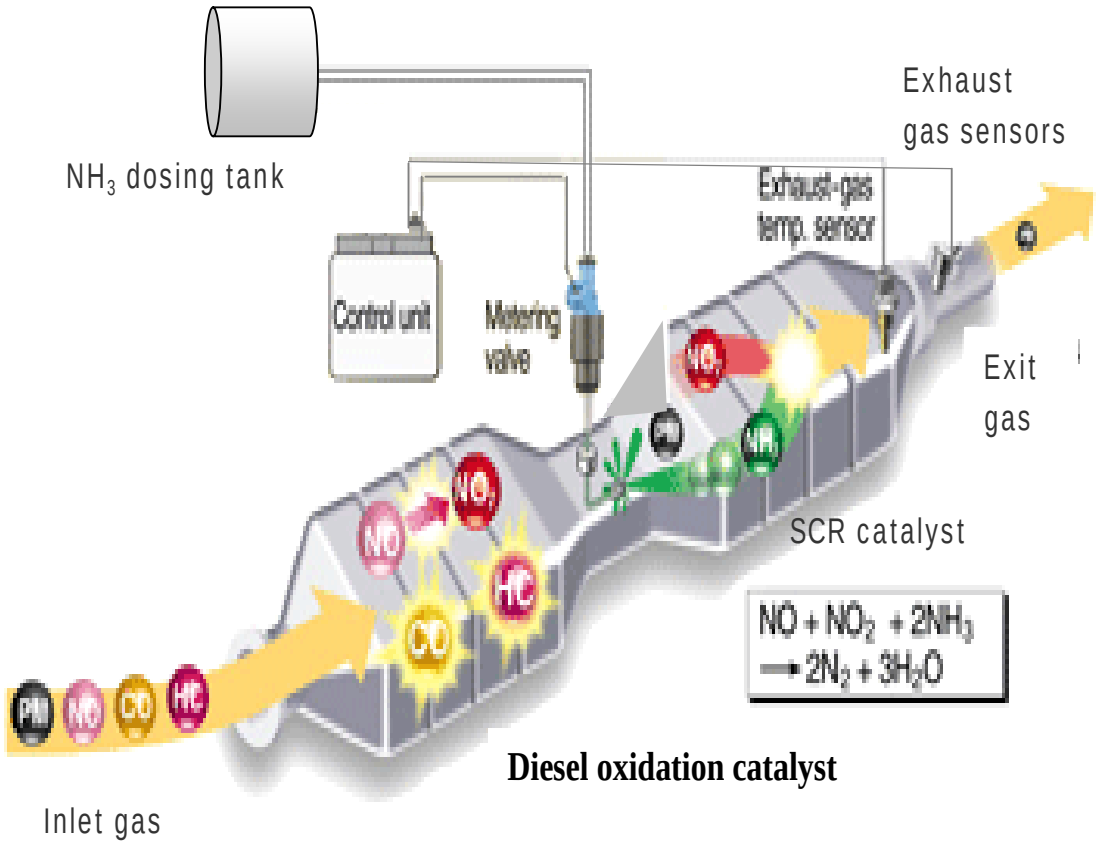

Figure 1-7: SCR system used for vehicle exhaust emission control [55]

1.7.2 Lean NO_X Traps

NO_X trap technology is the latest advancement in terms of removing NO_X species in the oxidizing environment of diesel engines. This emerging technology is basically a two step process.

First is the lean step where NO is catalytically oxidized to NO_2 and stored in an adjacent trapping site as a nitrate. The second step includes the conversion of trapped NO_X to N_2 using a reductant-rich exhaust, typically through a pulsed charge of fuel. The NO_X trap uses precious metals to carry out the NO to NO_2 and nitrates, and nitrates to N_2 conversion steps. An alkaline earth oxide component acts as the storage part for NO_2 to nitrates.

Therefore, NO_X trap operation can be categorized as a two-phase process, which includes a lean phase and a rich phase. The basic difference between the two phases is the gaseous ingredients that comprise each phase. At the laboratory scale we have created a simulated environment for a rich and lean phase. We use a mixture of gases as listed in Table 1-4 for each of the phases.

Table 1-4: Gaseous distribution along with time for each cycle

Phase	Time (s)	Gases				
Lean	60	CO_2 = 5%	H_2O = 5%	NO = 300ppm	O_2 = 10%	N_2 = balance
Rich	5	CO_2 = 5%	H_2O = 5%	H_2 /CO = 1%	O_2 = 1%	N_2 = balance

1.7.2.1 Lean Phase

The lean phase matches the normal exhaust of a diesel engine and consists of CO_2, NO_X, N_2, H_2O, particulates and O_2 etc. The O_2 content in diesel engine exhaust is high and it is difficult to reduce the NO_X into N_2 species in an oxygen rich surrounding. During the lean phase, any NO is converted to NO_2 due to the presence of the precious metal part of the

catalyst (platinum). This NO_2 is further oxidized to a nitrate species which is associated with the storage part of the catalyst (typically barium).

1.7.2.2 Rich Phase

Before the catalyst becomes saturated with nitrates, the air/fuel ratio is altered for a small interval of time (rich phase) in order to convert the trapped NO_X species and clean or regenerate the catalyst. To force the composition reductant-rich, the engine-in air content is lowered, so as to reduce oxygen in the exhaust. There is also an increase in the inlet fuel content to ensure enough reductant reaches the catalyst.

1.7.2.3 Time Interval for Each Phase

The time duration differs for each phase; usually the lean phase is longer, e.g. ~60 seconds, while the rich phase is shorter, and might occur for just few seconds. In practice, increasing rich phase time results in higher NO_X conversion, but also higher fuel consumption.

1.7.2.4 Catalyst

The catalyst used for these experiments is a platinum/barium/alumina catalyst. Each component has a specific function in relation to the reaction chemistry.

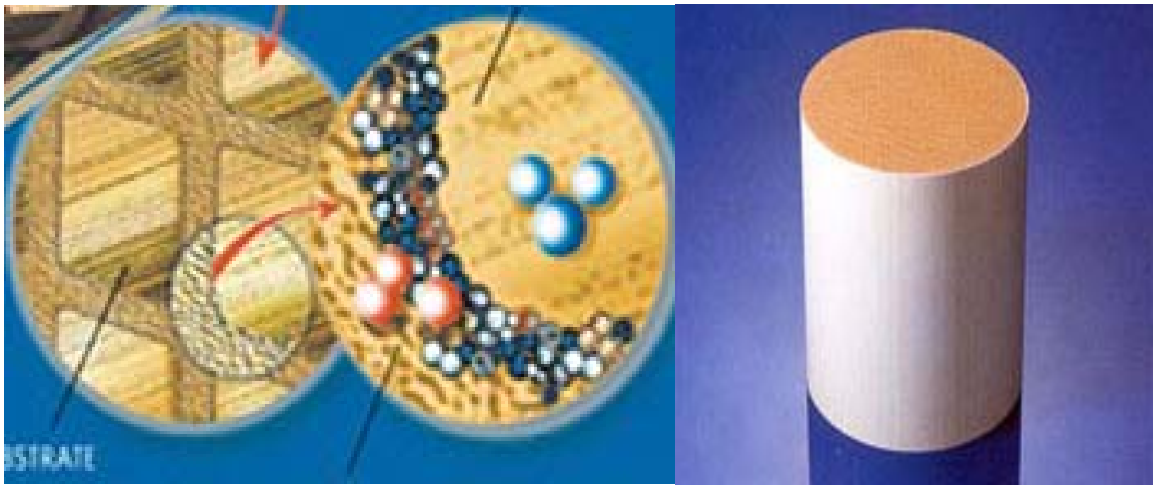

Figure 1-8: A ceramic honeycomb shaped catalyst block with a close up of its channels [56]

The catalyst is impregnated on an alumina wash-coat in a honeycomb ceramic block as shown in Figure 1-8 that provides maximum surface area for the gases to react. The catalyst component responsible for the redox reactions is platinum. The barium acts as the storage part of the catalyst. A more detailed description of the reaction steps will be discussed in a following chapter.

1.7.2.5 Summary

An overall objective in describing the various engine types, different catalyst technologies, emissions etc was to show how with each of these factors, there are efforts aimed at NO_X emissions control.

Chapter 2: Literature Review

One focus of this thesis is the reaction chemistry occurring on the NO_X adsorber catalyst and using temperature profiles obtained with IR thermography as a tool to investigate the reaction gradients on the catalyst surface. This chapter is divided into two main sections. The first section will focus on the reaction chemistry occurring on the catalyst surface while the second section will focus on the application of the IR thermography temperature measurement technique.

2.1 NO_X Traps- Reaction Chemistry Overview

NO_X trap reaction chemistry can be categorized into two main phases; the lean phase and the rich phase. In the lean phase, oxidation and storage of NO_X species on the catalyst surface occurs, while the reduction of stored NO_X species and catalyst regeneration is done during the rich phase. The data in Figure 2-1 describe one lean and rich cycle (data taken from our reactor).

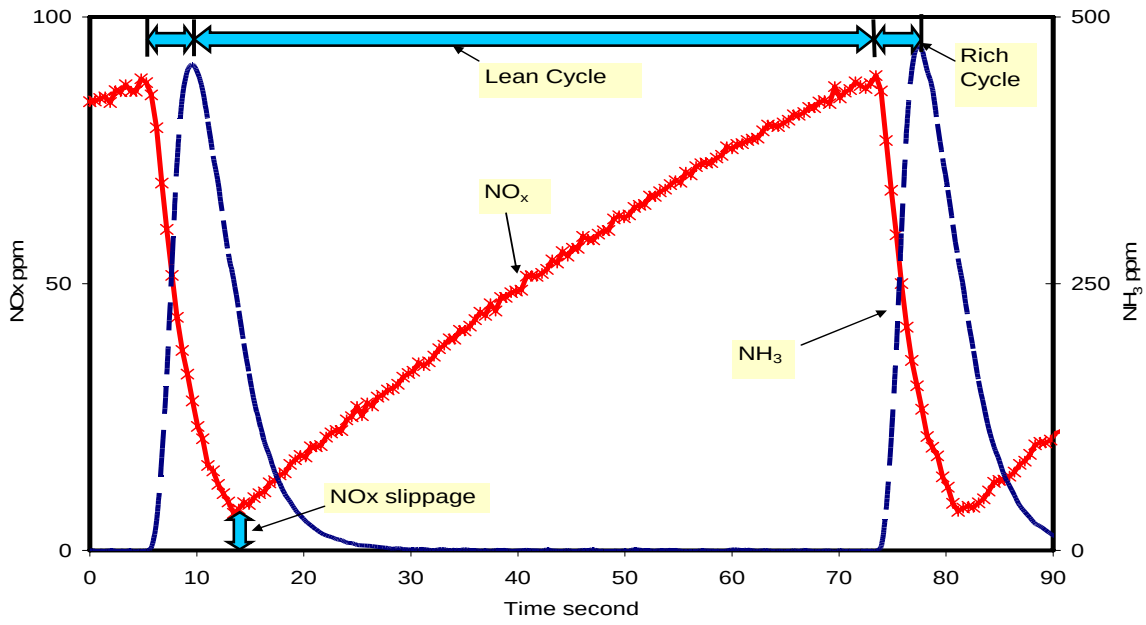

Figure 2-1: NO_X storage/release profile for a complete lean/rich cycle

The NO_X concentration during the lean phase rises gradually as the catalyst saturates while trapping NO_X over time. The NO_X concentration in the inlet stream remains constant throughout the lean phase of the cycle. The NO_X level in Figure 2-1 always remained above zero, full trapping for some period of time did not occur for this sample once a steady cycle-to-cycle performance was attained. This indicates that a small amount of trapped NO_X was already on the catalyst surface; or the previous regeneration was not sufficient to clean off the catalyst. After a minute, the phase was switched from lean to the rich phase for 5 seconds by the introduction of reductant H_2 /CO and the removal of O_2 and NO_X.

At that instant, two changes were observed. First, there was a sudden drop in the NO_X coming out in the exit stream because of its absence in the feed. Secondly, the NH_3 as a byproduct of NO_X to N_2 reduction appears as soon as the phase switches to rich. There was no ability to measure the N_2 concentration with the experimental apparatus used and therefore its formation during the rich phase cannot be shown. It is typically calculated with a mass balance, where the N_2 amount would close the balance. Such data indicate that NO_X trap has a finite capacity for NO_X storage but can be regenerated by switching to a rich gas-composition stream. Overall, this conversion from NO_X to N_2 is achieved in a five-step process described below [1].

1) NO oxidation to NO_2 (lean phase)
2) NO/NO_2 sorption on the catalyst surface (lean phase)
3) Reductant evolution (rich phase)
4) NO/NO_2 release from the sites (rich phase)
5) NO_X conversion to N_2 (rich phase)

The first 2 reaction steps occur during the lean phase while the other 3 are part of the rich phase. All steps are or can be catalytically driven. The failure of any individual step will significantly impair catalyst performance, as each reaction is interdependent. For better understanding of each step along with its performance parameters, the following discussion will be divided into 5 different sections.

2.1.1 Step1: NO Oxidation to NO_2 – (Lean Phase)

The initial step during the lean phase is the NO oxidation reaction. NO oxidation performance depends on several factors; thermodynamic/kinetic limitations, noble metal catalytic properties, its distribution on the catalyst and the combination of that noble metal with the type of alkali metal compound [1-4]. Overall, it is a difficult task to separate the oxidation step occurring on the surface from the adsorption step, as the product NO_2 can be trapped. The conversion of NO to NO_2 requires O_2 species adsorption on the catalyst surface which is temperature dependent. Previous research [2] has shown higher O_2 coverage for lower adsorption temperatures and desorption starting around 300°C. This limits the O_2 storage over the catalyst with temperature being the constraint. Thermodynamic equilibrium of NO and NO_2 as a function of temperature and O_2 concentration is shown in Figure 2-2. The calculated NO to NO_2 equilibrium data are based on thermodynamic predictions using Gibbs free energy calculations.

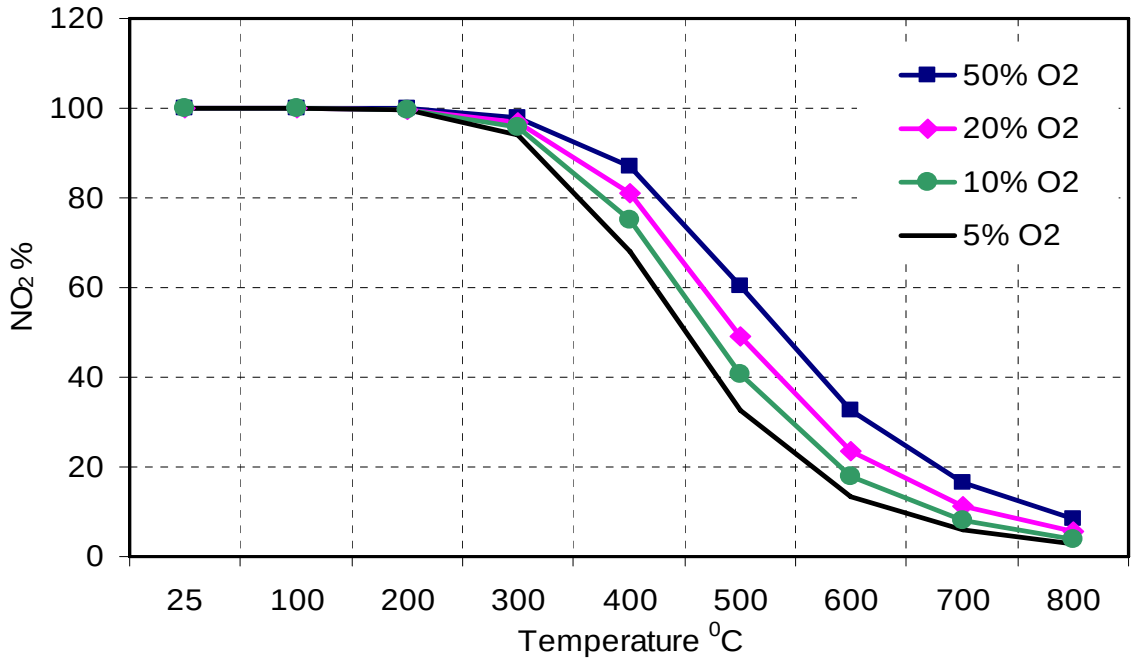

Figure 2-2: Thermodynamic NO/NO_2 equilibrium values where inlet gas contains 250 ppm NO_X, variable O_2 and the balance N_2

The thermodynamic limitations are not significant at temperatures < 200^{o}C. Thermodynamic equilibrium can influence the performance as the temperature is further increased. This trend is shifted to higher thermodynamic ranges by increasing the oxygen contents [1].

The performance of the catalyst of course relies on the ingredients that make up the catalyst. Pt is a common REDOX reaction catalyst component and is therefore a common component of NO_X trap catalysts. However, studies for the selection of another active oxidation component in the lean NO_X trap have been carried out. Unfortunately, however, the most common metals showing high performance for the oxidation reaction are the noble metals, Pt, Pd and Rh. A study [3] compared the performance of Pt and Pd, on a BaO-containing lean NO_X trap, while the wash coat was alumina in both the cases. A maximum 45% NO conversion was observed using the Pt-based catalyst at 230°C, while almost no NO oxidation was observed with the $Pd/BaO/Al_2O_3$ catalyst. Similarly, results from another study [4] comparing Pt with Rh, show Pt resulting in high NO oxidation activity during the lean phase both with and without SO_2 present in the gas feed, while Rh showed high activity for NO reduction in the presence and absence of $SO_{2,}$, indicating an increase in overall efficiency of the NO_X trap catalyst by combining Pt and Rh could occur. Overall, such evidence has made Pt the oxidation catalyst of choice [2-5].

It is also important to understand the kinetics of NO oxidation over Pt-based catalysts. A study has shown improvement in NO oxidation with lower Pt dispersion. The increased particle size was induced by high temperature sintering [5]. Another important kinetic limitation in NO oxidation is the space velocity, a measure of the residence time of a species in the reactor or monolith channel. Higher space velocity means higher volumetric gas flow rate or smaller catalyst volume. Previous data [1] support the idea that high NO to NO_2 conversion can be achieved more effectively at low space velocity or simply by allowing more residence time for the NO oxidation reaction to proceed. If NO_2 is in the lean phase along with NO, recent research predicts the NO oxidation reaction will be inhibited [6]. This rate inhibition by the product NO_2 is attributed to the fact that it has a high relative sticking coefficient so it keeps the Pt surface oxidized, and completely oxidized Pt is inactive.

The storage part of the catalyst does not play an active role in the oxidation reaction itself, but various studies indicate an effect of Ba on the reaction. A study comparing the performance of Pt/Al_2O_3 with $Pt/BaO/Al_2O_3$ shows a decrease in the NO oxidation reaction due to the presence of the Ba [2]. Possible reasons discussed include Ba covering the sites responsible for the oxidation reaction or it might be due to some kind of reverse spillover of NO_2 species from Ba to Pt i.e. movement of NO_2 species (by spilling rather than adsorbing on surface) back to Pt site close to Ba, due to more site availability resulting after decrease O_2 coverage on Pt [2].

2.1.2 Step 2: NO/NO_2 Sorption on the Catalyst Surface - (Lean Phase)

NO_X traps, as the name implies, rely on some trapping capability of the catalyst for performance. Stringent regulations on NO_X control will require significant trapping during the lean phase of the cycle. For $Pt/Ba/Al_2O_3$ catalysts, the Ba component is responsible for the sorption of NO_X species.

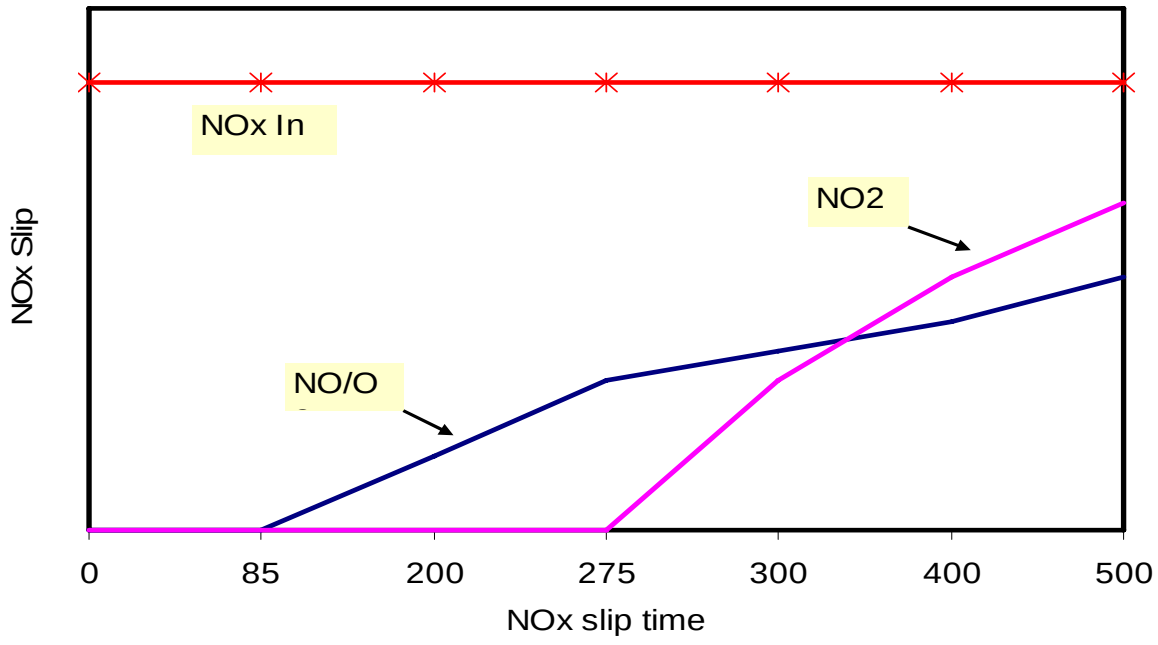

Figure 2-3: Outlet concentrations of NO_X species with NO and NO_2 in the feed stream on a $Pt/Ba/Al_2O_3$ catalyst showing trapping performance [1]

Work done by Hodjati et al. [41] and many other groups have shown that it is the NO_2 species that are trapped rather than NO. For example, the sorption performance is improved by changing from NO [1] or NO/O_2 [10] mixture in the feed to NO_2 as the NO_X source, as is shown in Figure 2-3. This improvement when using NO_2, amongst other factors, can also be attributed to the NO_2 being an oxidizing source for nitrate formation [2]. This improved trend even occurs at higher temperatures, where NO oxidation reaction is not the rate limiting step.

Various studies propose mechanistic models for the NO_X trapping process, where both NO and NO_2 sorbs to the sorption site. NO_2 or O_2 are both sources for O* species to form nitrates. Transport of NO and NO_2 to the sorption sites follows two possible pathways; either surface migration from the noble metal and then the formation of nitrates, or NO_2 formation and release from noble metal followed by re-adsorption on downstream sorption sites [1]. Mechanisms for NO_X trapping over a $Pt/Ba/Al_2O_3$ model catalyst listed in different studies [34, 35] are shown below.

Reaction involving Pt sites

$O_2 + 2Pt \rightarrow 2\ Pt\text{-}O$

$NO + Pt \rightarrow Pt\text{-}NO$

$NO_2 + Pt \rightarrow Pt\text{-}NO_2$

$Pt\text{-}NO + Pt\text{-}O \rightarrow Pt\text{-}NO_2 + Pt$

Reactions involving BaO sites:

$NO_2 + BaO \rightarrow BaO\text{-}NO_2$

$BaO\text{-}NO_2 \rightarrow BaO\text{-}O + NO$

$NO_2 + BaO\text{-}O \rightarrow BaO\text{-}NO_3$

$NO_2 + BaO\text{-}NO_3 \rightarrow Ba(NO_3)_2$

$2\ BaO\text{-}O \rightarrow 2BaO + O_2$

Other than the NO_X precursor discussed earlier, other gas-stream components also affect the adsorption step. O_2, H_2O and CO_2 are always part of lean-burn engine exhaust. A detailed study on the effects of these on NO_X storage with a Ba-containing catalyst was carried out [8]. Oxygen was shown to positively affect trapping, while CO_2 had a negative impact**.** The negative CO_2 impact on NO_X storage is quite evident at low temperatures; but seems to

disappear at elevated temperatures [37]. The H_2O content in the gas mixture can have a positive or a negative impact as its presence results in reduced trapping, similar to the CO_2 effect, over wide temperature ranges, but at the same time it reduces the negative CO_2 effect on the trapping. For example, the presence of H_2O significantly decreases nitrate formation on the Al_2O_3 component of the catalyst [9] via hydroxyl group formation, thereby blocking sorption sites. But, in the presence of H_2O, some $BaCO_3$ changes to $Ba(OH)_2$ on the surface which more readily forms nitrates [11]. The storage of NO_X occurs at BaO, $BaCO_3$ and $Ba(OH)_2$ species, with the first preference at BaO, then $Ba(OH)_2$ and then $BaCO_3$.

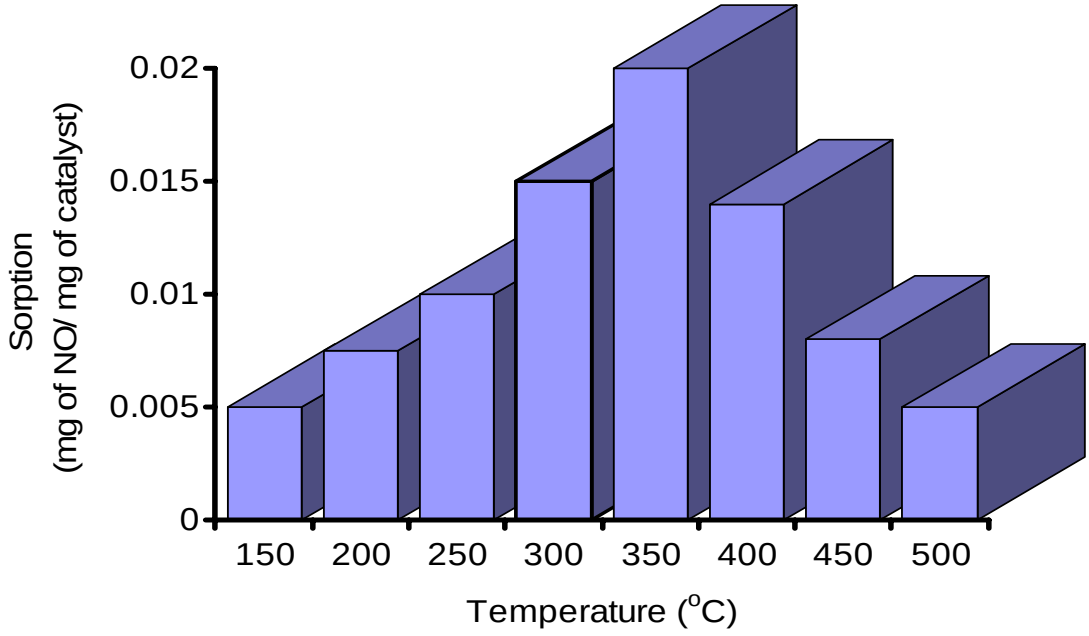

Figure 2-4: Temperature dependent NO_X adsorption trends [10]

Another important parameter affecting the sorption trends is of course temperature, as shown in Figure 2-4. Trapping shows a maximum in performance with temperature and a typical maximum in trapping capacity occurs at 350°C. As an increase in temperature until about 350°C results in an increase NO to NO_2 oxidation and increasing temperature increases diffusion rates from Pt sites to further trapping sites, both of these factors improve trapping

when increasing from low temperature. At temperatures higher than 350°C, the NO_2/NO ratio become fixed by the thermodynamic equilibrium between NO, NO_2 and O_2 species [10]. The poor performance at high temperatures is also attributed to decreased nitrate stability. Increased $Ba(NO_3)_2$ formation stops when the nitrate formation reaction is in equilibrium with the nitrate decomposition reaction.

The overall reaction chemistry during the first 2 lean steps is collectively shown in Figure 2-5. The catalyst shown is a standard $Pt/Ba/Al_2O_3$ catalyst showing the transformation of NO into stored nitrates on the Ba component of the catalyst.

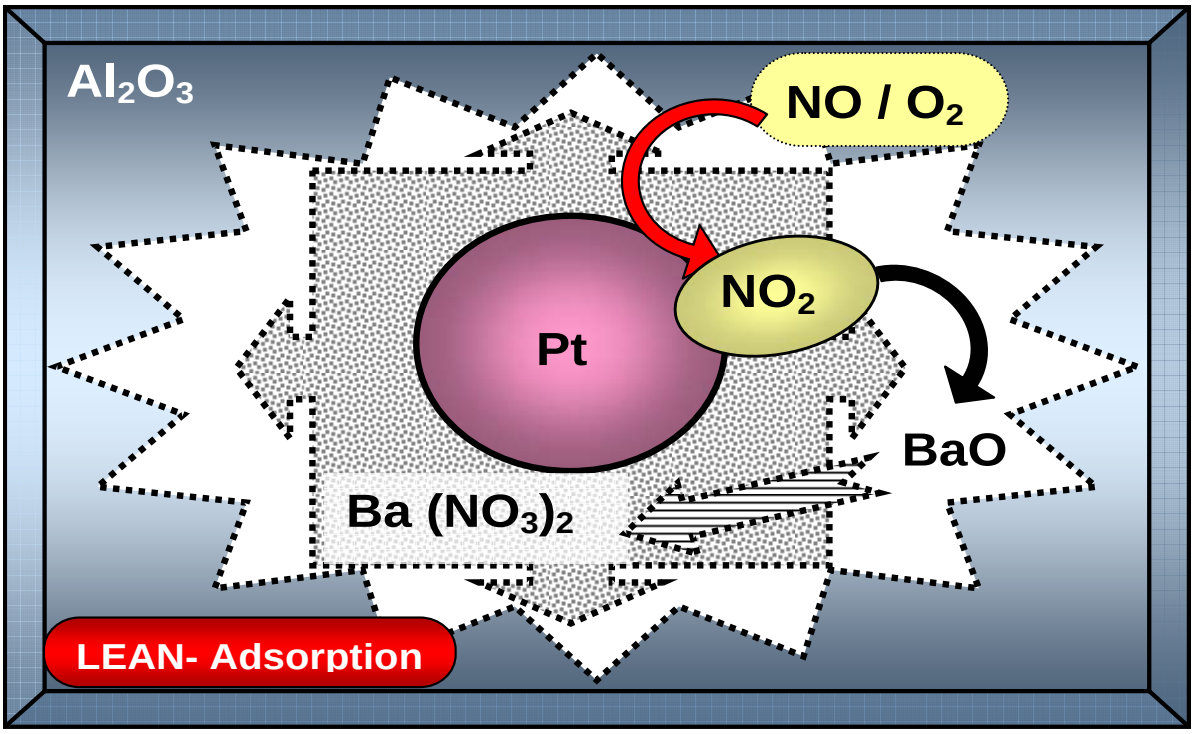

Figure 2-5: Lean phase reaction chemistry on a $Pt/Ba/Al_2O_3$ catalyst surface (steps 1-2)

2.1.3 Step 3: Reductant Evolution - (Rich Phase)

The third step occurs when the phase is switched from the lean to the rich phase. At that instant the oxygen concentration drops and a reductant is introduced, combining to form a reductant-rich gas mixture. The decrease in O_2 content obviously helps save some reductant for the NO conversion step rather than oxidizing to CO_2 and H_2O.

Various reductants have been tested, ranging from diesel fuel to CO/H_2 mixtures. Significant differences were observed when using the different types of reductant especially in different temperature ranges. Using CO even results in no performance at 150^oC [13].

Introducing the reductant has been accomplished in a few ways:

- First, the reductant (fuel) can be directly sprayed into the exhaust (in- pipe injection) upstream of the catalyst [22].
- The second is fuel injection and processing over a partial oxidation or reforming catalyst located upstream of the NSR catalyst. The fuel is converted by this upstream catalyst to better reductant (H_2) [1].
- Third, and seemingly the most desired and most common, is the periodic delivery of the reductant from the engine itself.

CO and H_2 are considered better reductant than hydrocarbons [1] and therefore the in-cylinder regeneration strategies developed for lean NO_X traps target production of H_2 and CO. Fortunately, results from a previous study show that fuel chemistry does affect engine out hydrocarbon species types and amounts but shows no effect towards the CO or H_2 amounts in the outlet stream during rich exhaust production [22].

2.1.4 Step 4: NO/NO_2 Release from the Trapping Sites - (Rich Phase)

With the introduction of the rich pulse, the reductant contacts the catalyst surface resulting in NO_X release followed by its conversion. The release and conversion steps are overlapping but will be explained separately. The release of unconverted NO_X can be seen as an increase in NO_X concentration at the onset of the rich phase, as shown in Figure 2-6.

Various factors influence this release, including temperature, catalyst composition and thermal aging. Data from past work suggest that the NO_X released from the front of the catalyst also gets readsorbed on downstream sections of the trap [23] complicating analysis. The difference in NO_X release patterns with changing temperature in different studies is due to the different compositions of gases in contact with the catalyst surface. However, there is a general consensus on the effects of temperature on the chemistry, if not the rates. At low temperatures (for example at 250^oC and below) the release is dependent on the catalyst's

ability to activate the reductant, so an increase in temperature improves NO_X reduction resulting in a decreased unconverted NO_X release.

At temperatures nearer 350°C, a source of NO_X release is the heat generated from various oxidation/reduction reactions. The reductant can react with oxygen to generate local temperature exotherms. These exotherms raise the temperature on the catalyst surface, hence affecting the thermodynamic stability of NO_X resulting in its release [23].

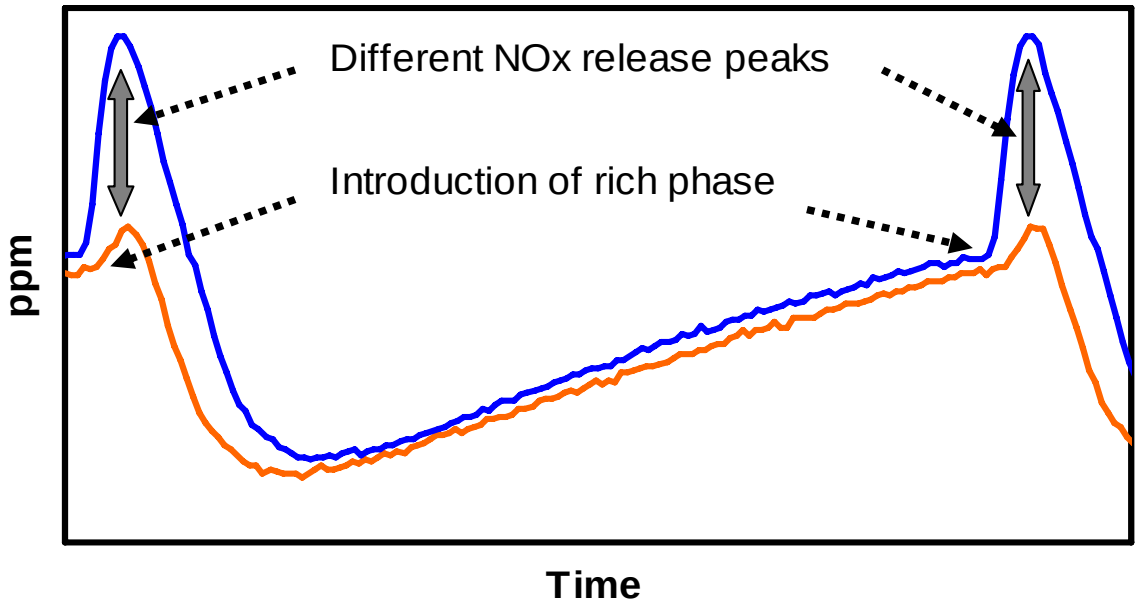

Figure 2-6: Comparing release peaks at the start of the rich phase for different runs

At elevated temperatures, for example near 500°C, high nitrate instability leads to rapid nitrate decomposition and NO_X release from the catalyst [23]. Furthermore, the nitrate stability depends on the type of reductant used and its efficiency for reduction. The nitrate stability on a Pt/Ba-based model catalyst decreased when the reductant was changed from propane to CO to H_2 [36]. Research [13] has also shown an NO release peak in the absence of water with H_2 as the reductant at lower temperatures and with CO at higher temperatures. In that study, the largest NO release peak was observed with H_2 at 150°C. The reason for this sudden unconverted NO release is NO failure to dissociate at low temperatures.

Even with the larger release peaks during the rich phase when using H_2, its use has consistently shown improved overall behavior compared to the other reductants as there is greater extent of catalyst regeneration [1]. CO as a reductant can either directly react with NO or provides hydrogen as the reducing agent via the water gas shift reaction [1]. Continuing with the general theme that H_2/CO mixtures would be better than larger hydrocarbons, work [47] using on-board fuel reformers as a potential way to generate H_2 for the after treatment system has shown promise.

The lean phase time also has a direct impact on the NO_X release, as an increase in lean phase time means more NO_X is deposited on the surface which in turn would result in higher NO_X release peaks if the same amount of reductant is always added [23]. Overall, the amount released is still a function of the reduction and release rates.

2.1.5 Step 5: NO_X Conversion to N_2 - (Rich Phase)

The final step in the NO_X storage and reduction chemistry is the conversion of released NOx from the surface of the catalyst into N_2 during the rich pulse. Therefore, the overall objective will finally be achieved. The primary factors affecting the reduction step include type of reductant, amount of reductant, catalyst composition and temperature [1, 13-15]. For example, the effect of the amount of reductant has been studied where improvement in reduction was observed with increasing the CO content as well as rich phase time [1].

Other than these factors, the catalyst composition also has an effect as previous work [14] has demonstrated improved reduction performance in the presence of Na as an added component to a Pt-based catalyst. The alkali presence increases the NO adsorption on the catalyst resulting in more available surface N species for conversion to N_2 [14]. The same trends have been confirmed when Ba was added instead of Na [42].

Literature suggests two possible reaction mechanism pathways for NO reduction to N_2. The first suggests that NO sorbs on reduced Pt, which reduces the NO to N which finds another N to form N_2. But then these Pt sites are now oxidized and inactive. The reductant introduced in the rich phase then reduces the Pt sites by acting as a scavenger for O species on the Pt-O sites. This reduced Pt is then active again [15]. The second pathway suggests a direct reaction between NO_2 and the reductant following an adsorption, conversion and desorption

Langmuir-Hinshelwood pathway. The study [22] proposed the presence of intermediate products (organic nitro species) on the catalyst surface, and these organic nitro species behave as the reaction intermediate and contribute to the catalytic formation of N_2 and N_2O.

The selection of the noble metal catalyst component is also important for the reduction reaction. In comparing the performance of platinum-group metals, both Pt and Rh show high NO conversion to N_2 at temperatures ranges from 200 and 350°C [16].

In the above paragraph, the reductant used in the different studies was hydrocarbons, but the behavior of other reductant species such as CO or H_2 follow the same trends. The improvement in catalyst performance in terms of decreased NO_X release peaks using H_2 as a reductant at moderate operating temperatures was discussed earlier; this effect is due to an improvement in reduction performance relative to other reductants [13]. But, as the temperature is increased, the performance improvement with H_2 decreases. At low temperature, some studies show CO acting as a poison for the Pt sites thus hindering the release and reduction process on the catalyst surface [19]. In another study where diesel fuel was compared with a CO/H_2 mixture and H_2, diesel fuel showed a 5%, CO an 81% and the CO/H_2 mixture a 95% NO_X conversion efficiency at temperatures below 200^{o}C but at higher temperatures this performance improved to 80% for diesel fuel and simultaneously for the CO and the CO/H_2 mixture it went to 100% [20].

The NO reduction reaction ideally results in the formation of N_2 but it can follow other reaction pathways resulting in the formation of byproducts like NH_3 or N_2O [1]. The formation of both these byproducts increases with an increased amount of reductant. A study [24] has shown that below 200^{o}C with H_2 and/or CO as the reductant, formation of all three product species (N_2, NH_3 and N_2O) was seen, but at higher temperatures, the reaction becomes more selective towards one or two of the three products. In the same study with H_2 as the reductant, NH_3 formation was increased in comparison to when CO was used. NH_3 formation is temperature-dependent, where it decreases with decreasing temperatures from 350°C [13]. The amount of reductant to make the different products varies; the reaction between CO and NO producing N_2 requires 2 moles of CO as compared to 1 mole of CO for conversion of NO to N_2O. That means if the NO reduction reaction forms N_2O instead of N_2,

the CO could become in excess and therefore be released. With NH_3 formation, more reductant is consumed than is required for N_2 formation. This deficit could leave the catalyst not fully regenerated [24].

The presence of O_2 can also affect the NO reduction reaction as it is very difficult to achieve NO reduction in an oxygen-rich environment. As stated above, Pt is an active catalyst site for the NO decomposition reaction. According to the first mechanism discussed, during NO dissociation the N species recombine and leave the surface while leaving O species to react with reductant and be removed from the surface. Excess O_2 would mean more reductant is needed to reduce the Pt-O sites, which can now also form from the gaseous O_2. However, if hydrocarbons are used as the reductant source, carbonaceous species can form, and the oxidative removal of carbonaceous species from active Pt sites helps [21]. And as mentioned above, the presence of O_2 would result in reaction with the reductant, which is an exothermic reaction generating heat and therefore accelerating release. Accelerated release, without a proportional accelerated reduction rate could result in less overall reduction.

The overall reaction from steps 3-5 is summarized in Figure 2-7, using a $Pt/Ba/Al_2O_3$ catalyst, and CO/H_2 as the reductant.

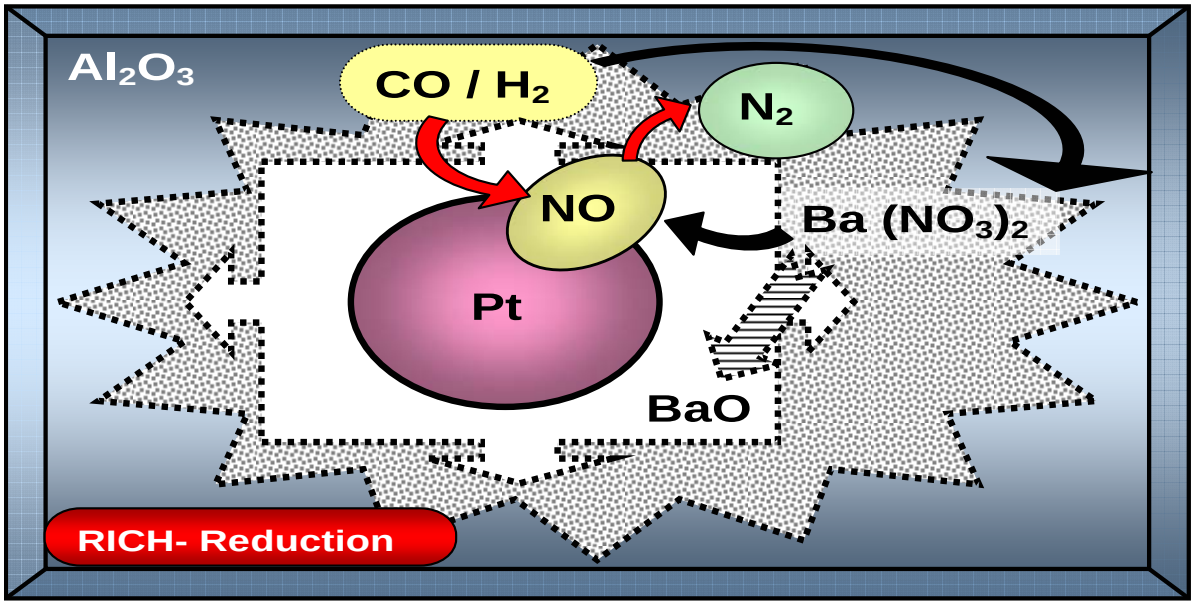

Figure 2-7: Rich phase reaction chemistry on a $Pt/Ba/Al_2O_3$ catalyst surface (steps 3-5)

2.2 IR Thermography

Various techniques are used to measure temperature, and these measurement techniques in terms of the type of contact between the measuring device and the medium of interest can be classified into three categories.

- Invasive – the measuring device and medium of interest are in direct contact, e.g., a thermocouple.
- Semi-invasive – the medium of interest is treated to enable remote observation, e.g., surface coatings to show color changes with temperature.
- Noninvasive - the medium of interest is observed remotely, e.g., infrared thermography.

Using a noninvasive method, high temperatures or chemical reactivity constraints of the medium will not influence the measuring technique being used [26]. A noninvasive technique that uses the relative measurements of infrared thermal radiation energy is called infrared thermography (IRT). Thermal radiation is a continuously emitted type of electromagnetic radiation by all substances [27]. It results due to molecular and atomic agitation associated with the internal energy of the material. Any object emits energy proportional to its surface temperature. However, the energy detected by the infrared camera also depends on the emissive coefficient of the surface under measurement.

Sensors like thermocouples are considered zero dimensional; they yield the local heat flux at a single point. This constraint makes experimental work difficult whenever heat flux fields exhibit high spatial gradients. In this context a two-dimensional infrared thermography technique is particularly helpful as an accurate surface temperature measurement that can map the presence of relatively high spatial temperature gradients [28]. With thermography, there is also flexibility in choosing an area of interest, along with optional further processing and analysis of the collected data. Overall thermocouple measurements in comparison to Infra red thermography are localized and do not reflect temperature distributions that might exist over catalysts [32].

An infrared imaging system can provide both qualitative and quantitative measurements. Heat values generated (temperatures measured by IR thermography) on a surface are related

to convective and conductive heat transfer [29]. From such data the temperature generated can be used to measure the heat transfer coefficient in forced and natural convection both for laminar and turbulent flow regions. In our experimental work, all three modes of heat transfer were present: conduction along the surface, convection in the gas-phase, and, of course, radiation heat resulting in image formation.

Infrared thermography in the area of catalysis has been mostly used for screening of active catalytic materials: monitoring time-resolved heterogeneous catalytic reactions, recording oscillating behavior in some reactions, and generating thermal images of dynamic surfaces. One such study (40) successfully identified localized areas for non-uniform activity on a catalyst surface. Combined with mass-spectrometry, the study showed oscillations in the rate of propane oxidation to synthesis-gas over metallic nickel were accompanied by periodic temperature changes on the surface.

Another study (31) showed that for a catalytic CO oxidation test there was a difference in the data collected using FTIR and IRT techniques. The FTIR technique measured the average CO adsorption over a particular area but was unable to spatially resolve the adsorption to the extent of IRT. The use of IRT made it possible to show the dynamics of both the temperature and spatio-temporal concentration patterns during CO oxidation [31]. The use of IRT was also found helpful in tracking the propagation of thermal fronts and their effect on oscillations that are observed in the catalytic oxidation of CO under unsteady feed conditions on supported Rh and Pt catalysts [39].

A similar work by Li et al. [38] used an indirect change in temperature measured by IRT as a tool to compare activities between catalysts with different combinations of metals at different temperatures in a parallel flow reactor. Small temperature change values were useful in indicating major trends and helped choose the more active samples. This work is similar to our project, where we use the IRT technique as an indirect measurement technique and combine it with gas analysis in order to create a bridge between the heat generated and the position of product formed on the catalyst surface.

Chapter 3: Experimental Work

3.1 Experiment Description

3.1.1 Gas- Mixing & Heating Section

The experimental objective was to create a simulated diesel engine exhaust environment while adjusting key process variables and monitoring the effects on the reaction, by means of IR thermography. The simulated exhaust gas is made using bottled gases provided by PraxAir. The individual gas flows to the reactor system are controlled and monitored using mass flow controllers. These controllers are themselves controlled via a labVIEW program, so that a specific gas mixture composition can be calculated and set. The gases used for these experiments include N_2, O_2, CO_2, NO, NO_2, CO and H_2. H_2O was also added, but in a heated zone downstream of the flow controllers.

As detailed earlier, in NO_X Storage/Reduction Catalyst (NSR) operation there are two phases of operation, lean and rich, where the lean phase is normal diesel engine operation and the rich phase is imposed to regenerate the catalyst. Therefore, for these experiments two separate manifolds were used: one for the rich phase and the other for the lean phase. These two phases do not mix prior to entering the system. The two manifolds are each attached to a four-way pneumatic switching valve. One stream goes to the reactor, the other is simply vented. A common gas mixture and distribution scheme is shown in Figure 3-1.

The speed for switching the valve between the flows is less than 1 second (advertised by the supplier Whitey Co/Swagelok as <100 ms). Switching can be manual or computer controlled. Once the gas mixture exits the four-way valve, it is run through a pre-heating section to raise the temperature so that H_2O can be introduced. This is the first heating zone for the gases entering the system. Usually the gases are heated to approx 200°C. A separate water injection system along with its controllers is used to inject water into the process stream. This water injection system performs controlled evaporation. The complete system consists of liquid and carrier gas flow controllers and a temperature controlled mixing and evaporation device.

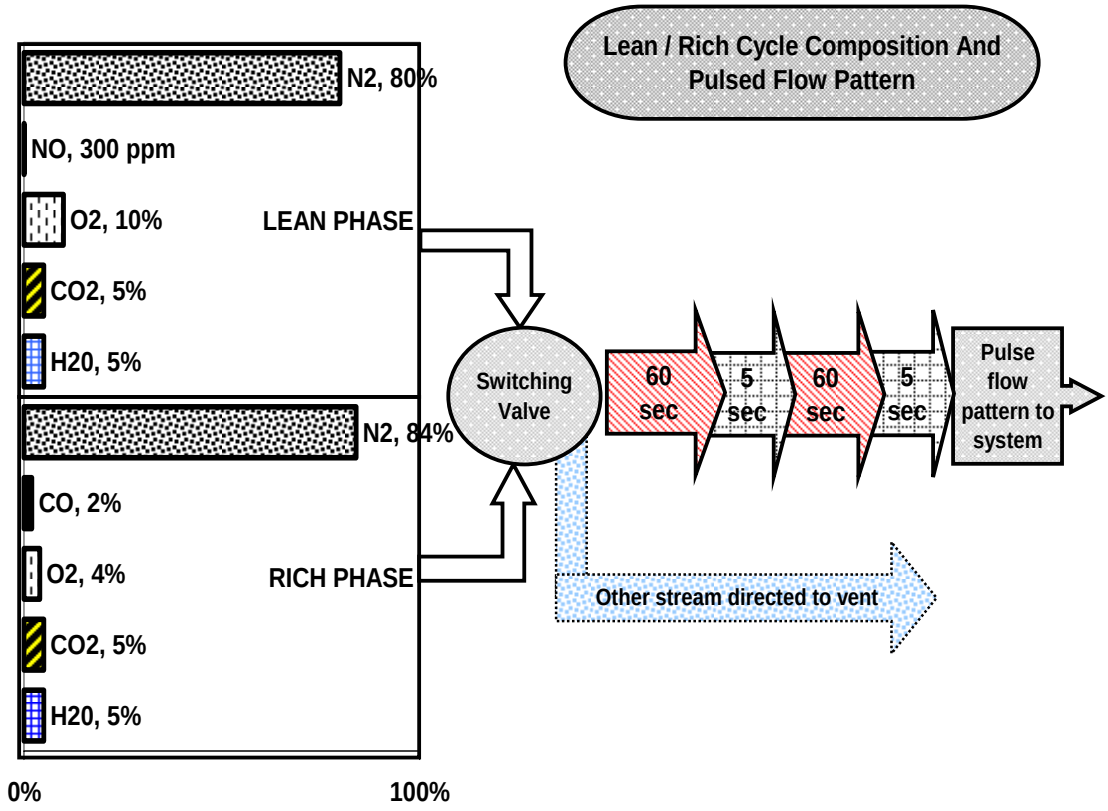

Figure 3-1: Lean/rich phase time control for the reactor

Our water injection system uses nitrogen gas as the carrier. An additional heater is also provided with the water injection system to heat the exiting water vapor up to 200^{o}C before entering the system. The gas mixture then passes through a high capacity pre-heater, which increases the gas temperature to a targeted temperature value, which in our experimental work ranges from 200-600°C. The basic design of the pre-heater is simply coiled tubing enclosed in an electrical heater. The coiling provides enough residence time for the gas mixture to attain the desired temperature. Once the desired temperature is reached, it is maintained in the reactor by means of custom-made ceramic heaters that surround the reactor. All the heaters are electric resistance type heaters and all the tubing between each heater is heavily insulated to prevent as much heat loss as possible.

3.1.2 Reactor & Catalyst Section

The reactor is a stainless steel block designed and custom-manufactured to provide a specific flow path for the gases to the catalyst. The catalyst sits in the middle of the reactor block. A picture of the reactor is shown in Figure 3-2. The square hole in the top of the reactor allows a view of the catalyst surface for temperature measurements via IR thermography technique during experiments. This hole is sealed with an IR transparent sapphire window. A sapphire window was used rather than other types as it can handle the high temperatures and gas compositions used. There are special openings provided in the reactor which are used to place thermocouples inside the catalyst bed. The catalyst sample used in these experiments was composed of Pt and Ba on an Al_2O_3 washcoat, all coated on a cordierite monolith.

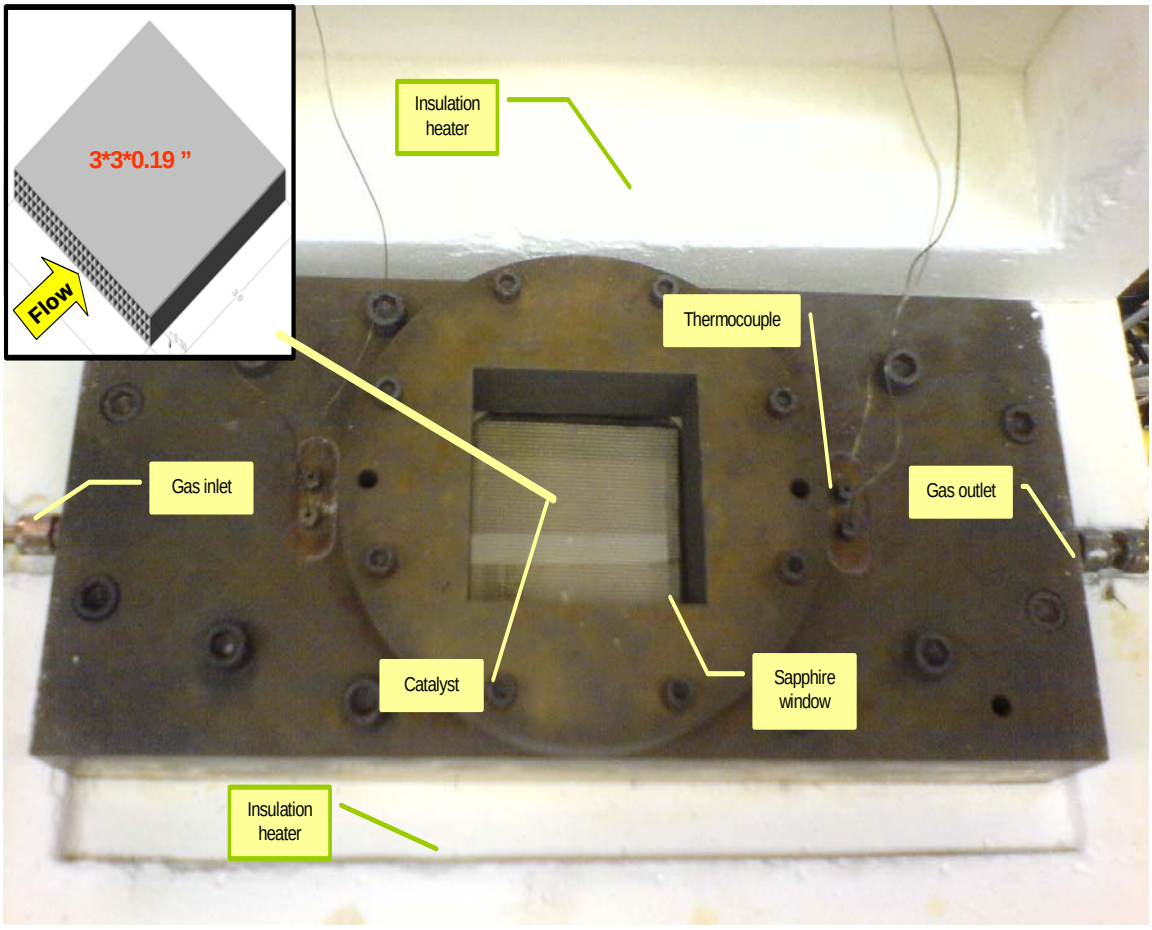

Figure 3-2: Reactor housed in the insulation box. Inset- 3-D cut catalyst sample view

Details regarding the reactions occurring on the catalyst were described in the previous chapter. The catalyst sample used was cut from a honeycomb monolith catalyst block, provided by Johnson Matthey. The catalyst length and breadth were kept constant from sample to sample, each measuring $3^{//}$ by $3^{//}$ in width and length. The catalyst height was altered by adding or removing a layer of cells (channels) from the sample to obtain the desired catalyst sample volume.

3.1.3 Gas & Reaction Analysis

Fourier Transform Infrared (FTIR) spectroscopy was used for gas analysis. This technique is based on each chemical functional group absorbing light at specific frequencies, and measuring the amount absorbed. The FTIR measurement technique includes comparison between unknown and standard spectra within a vendor-supplied database to identify the material being analyzed; quantitative analysis is performed for each compound in characteristic regions of its IR spectrum. The FTIR spectrometer was a MKS MultiGas ™ 2030, a high-resolution gas analyzer. It is able to measure concentrations of CO, NO, CO_2, NO_2, SO_2, O_2, various hydrocarbons, H_2O, NH_3 and N_2O gases in less than a second. From the gas analyzer, all the exit gases were directed to the building exhaust.

Reaction analysis was further evaluated using infra-red (IR) thermography. IR cameras have the ability to measure infrared energy emitted from an object and translate this directly to temperature. As the source temperature goes up so does the IR radiation emitted. The IR camera produces images of infrared radiation from the object and provides precise, non-contact temperature measurements. The camera used was the Merlin ^{TM} Mid IR camera made by FLIR. Some of the features include:

- a 320-256 focal plane array format for image resolution;
- an image collection frequency of 50 Hz;
- a measurement range from 0^oC to 2000^oC; and
- a sensitivity to temperature of 0.018^oC.

For temperature verification and for upstream temperature confirmation, thermocouples were used. The thermocouples were J-type purchased from Omega^{TM}.

3.1.4 Experimental Procedure

The overall reactor diagram/schematic is shown in Figure 3-3.

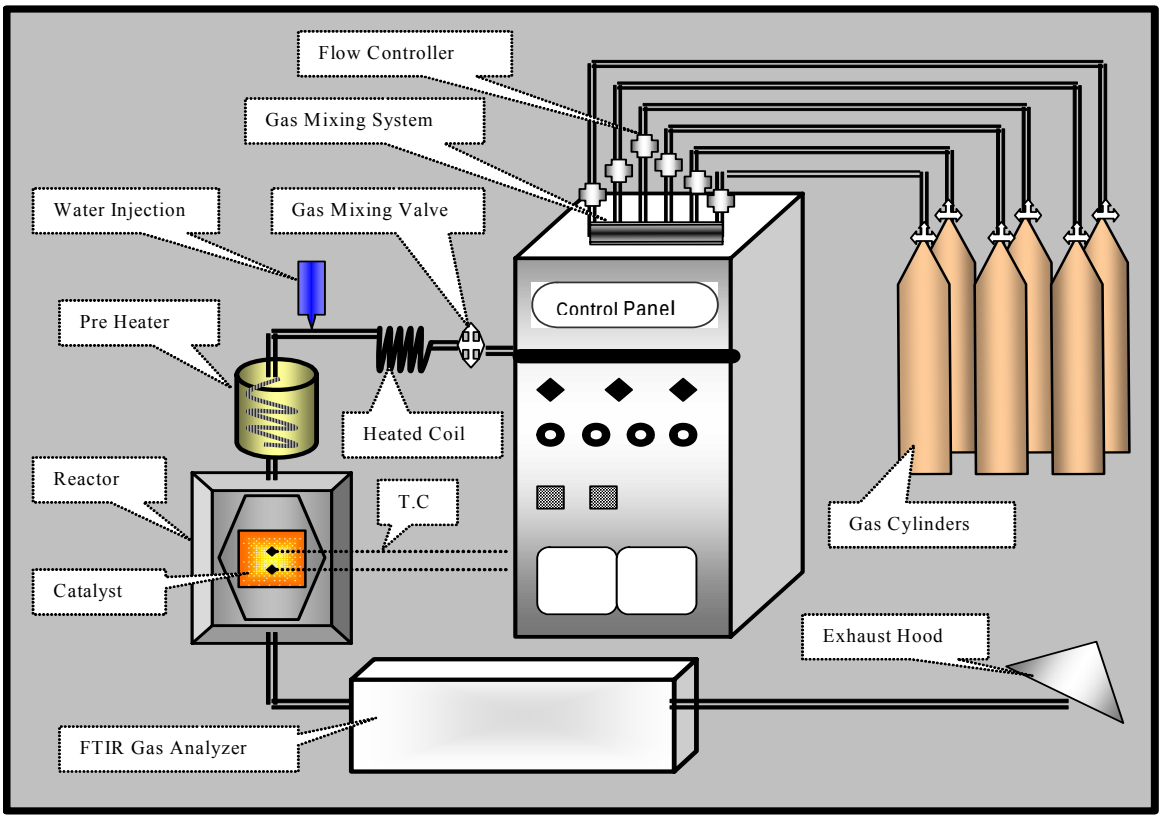

Figure 3-3: Complete process flow diagram

Overall, the targeted gas mixture is made using the mass flow controllers. These gases are then heated up to a desired reaction temperature in a step wise sequence using the pre-heaters. The catalyst surface temperatures while reactions taking place at a particular reaction temperature and gas composition are measured by the IR radiation intensity. The performance is further described by measuring exit gas concentrations. The outlet gas concentrations give an estimate of the extent of conversion taking place on the catalyst surface. The temperature changes observed indicates the extent and location of reaction on the catalyst. The data recorded with the IR camera is in a form that needs to be transformed to temperature data.

3.2 Image Transformation

The camera is placed vertically over the reactor and takes images of the catalyst surface through the sapphire glass window. The first step involves the transformation of the actual surface image to a colored image palette by the camera.

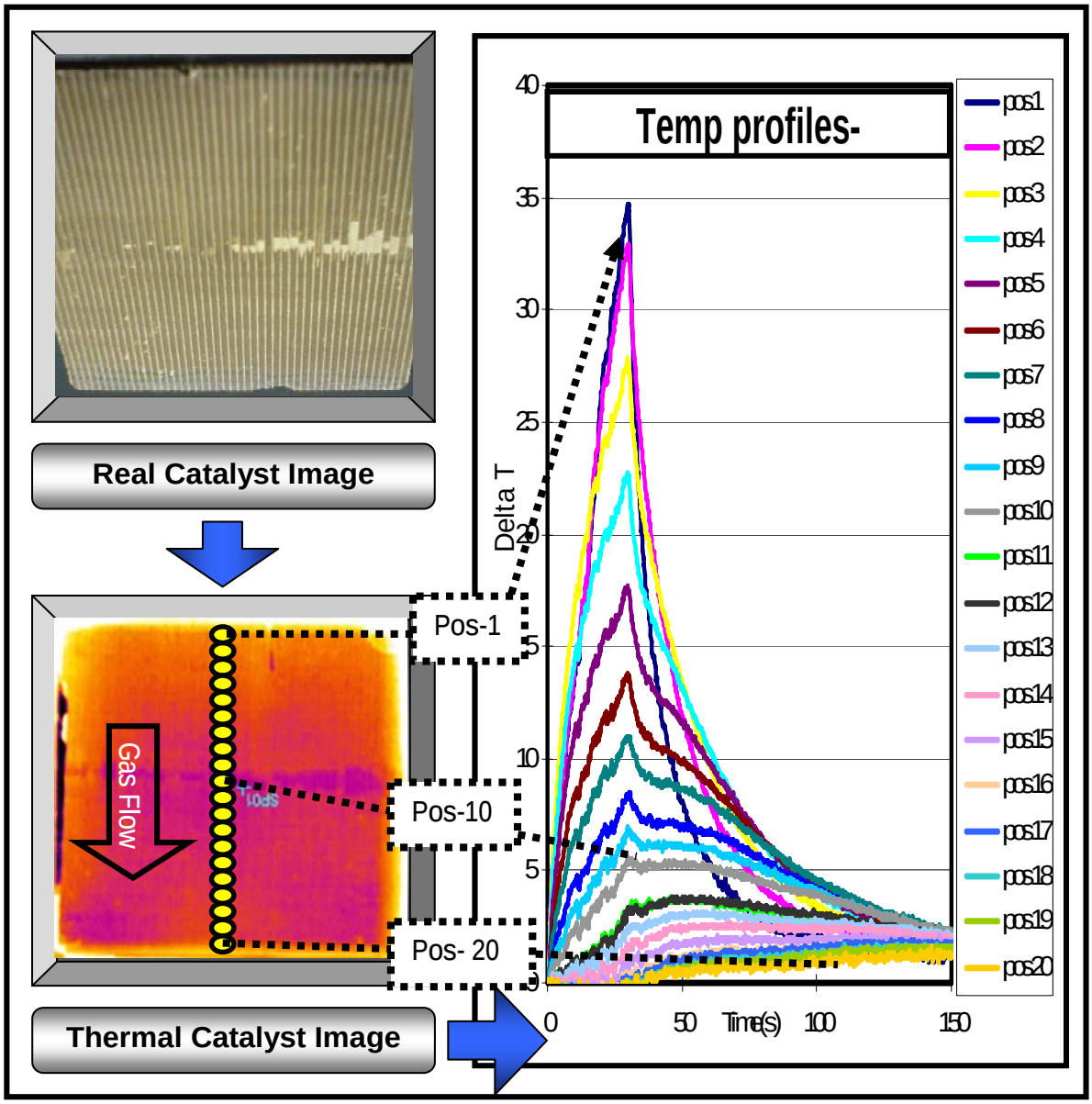

Figure 3-4: Representation of the conversion of a real catalyst image to the temperature profiles

The camera converts radiated heat energy from the catalyst surface into an electrical signal which is then displayed on the monitor as real-time data for recording or analysis. The camera uses different color palettes for showing various temperature zones in an image, see Figure 3-4. In the second step, using vendor-provided software, ThermaCam Researcher ™, the color palette is transformed into temperature. The data analysis can include spot measurements, axial/radial lines of temperature profiles, or area histograms etc. In the experiments for this work, a radially centered axial line from inlet to outlet was used and on that axial line 20 equidistant area histograms for temperature measurements were extracted. In this manuscript, pos1 is the radial-central catalyst inlet, pos 10 the radial and axial middle and pos 20 is the radial-central outlet of the catalyst.

In order to make analysis easier, rather than plotting actual temperatures versus time, we convert the temperature scale into a change in temperature for analysis. The change is based on the catalyst temperature before the start of the experiment, which is used as the initial temperature reading. The change in temperature should therefore represent any temperature development via any exothermic or endothermic reaction occurring on the surface. An example of the temperature changes calculated with the introduction of a rich phase, resulting in an exothermic reaction between the reductant with the surface oxygen and nitrate species is shown in Figure 3-4. In this specific experiment the highest temperature change occurs at position 1 and the temperature decreases down the length of the catalyst.

3.3 Types of Experiments

Three different sets of experiments were conducted. The first experiment was a base-line experiment, the purpose being to observe the extent of participation of the reactor itself as a catalyst during the course of the tests. The start of run temperature was kept at 300 or 400^{o}C with 250 ppm of NO entering during the lean phase. Four percent CO was introduced into the rich phase as the reductant. The lean and rich phase times were 50 and 10 seconds respectively.

The second experiment was also run at both 300 and 400^{o}C catalyst inlet temperatures. The purpose of this set of experiments was to monitor the effect of different oxygen

concentrations in the rich phase on the performance of $Pt/Ba/Al_2O_3$ catalyst. The experiment was run with three different oxygen (0, 2 and 4%) concentrations in the rich phase, while keeping the amount of reductant, CO in this case, constant at 4% in all three runs. The cycle time was 60 and 8 seconds for the lean and rich phases respectively.

The third set of experiments was to observe the spatial gradients of trapped NO_X on the surface of the catalyst. The lean phase time was increased until the catalyst was completely saturated. On introduction of the rich phase, having 1% H_2 and no O_2, the temperature gradients formed on the catalyst surface were analyzed. This allowed evaluation of the position of NO_X deposited on the surface. This experiment was run at 300 and 400^oC while using both NO and NO_2 in the lean phase. The average starting temperature for the 400^oC experiments read as 400^oC by the thermocouple, but 430^oC by the IR camera. This difference is due to the calibration span of the camera in that range.

Chapter 4: Results & Discussion

In order to demonstrate axial temperature gradients during operation and NO_X concentration profiles on a NOx adsorber catalyst, three sets of experiments were conducted. The first was a baseline experiment to verify that the reactor itself does not play a role in the reaction. The second set of experiment was done to examine the effects of oxygen addition to the composition of exhaust gas during the rich cycle on performance and catalyst temperature. The third set of experiments was conducted with no oxygen in the rich phase so all the reductant was free to react with the NO_X on the surface, isolating the nitrate reaction chemistry during regeneration on the catalyst.

4.1 Experiment Set 1: Reactor Effects

4.1.1 Objective

Determine any effect of the reactor on gas composition.

4.1.2 Experimental Setup

Table 4-1 lists the experimental conditions used in this series of experiments.

Table 4-1: Experimental conditions to evaluate reactor participation in the reactions

Flow (L/min)	12	**Catalyst**	Pt/ Ba/ Al_2O_3	**Sp.vel (hr^{-1})**	30000	**T (^oC)**	300/400
Composition	**H_2O**	**CO_2**	**O_2**	**NO**	**CO**	**N_2**	**Time (s)**
Lean phase (%)	0	0	8	250 ppm	-	Bal	50
Rich phase (%)	0	0	1	-	4	Bal	10

4.1.3 Results & Discussion

Ideally, the gas composition measured at the reactor outlet should show square waves with switches in inlet gas composition and there should be no composition changes at steady-state flow when the reactor is empty. However, as shown in Figure 4-1, the results obtained at 400°C differ slightly from the ideal case in terms of a square wave.

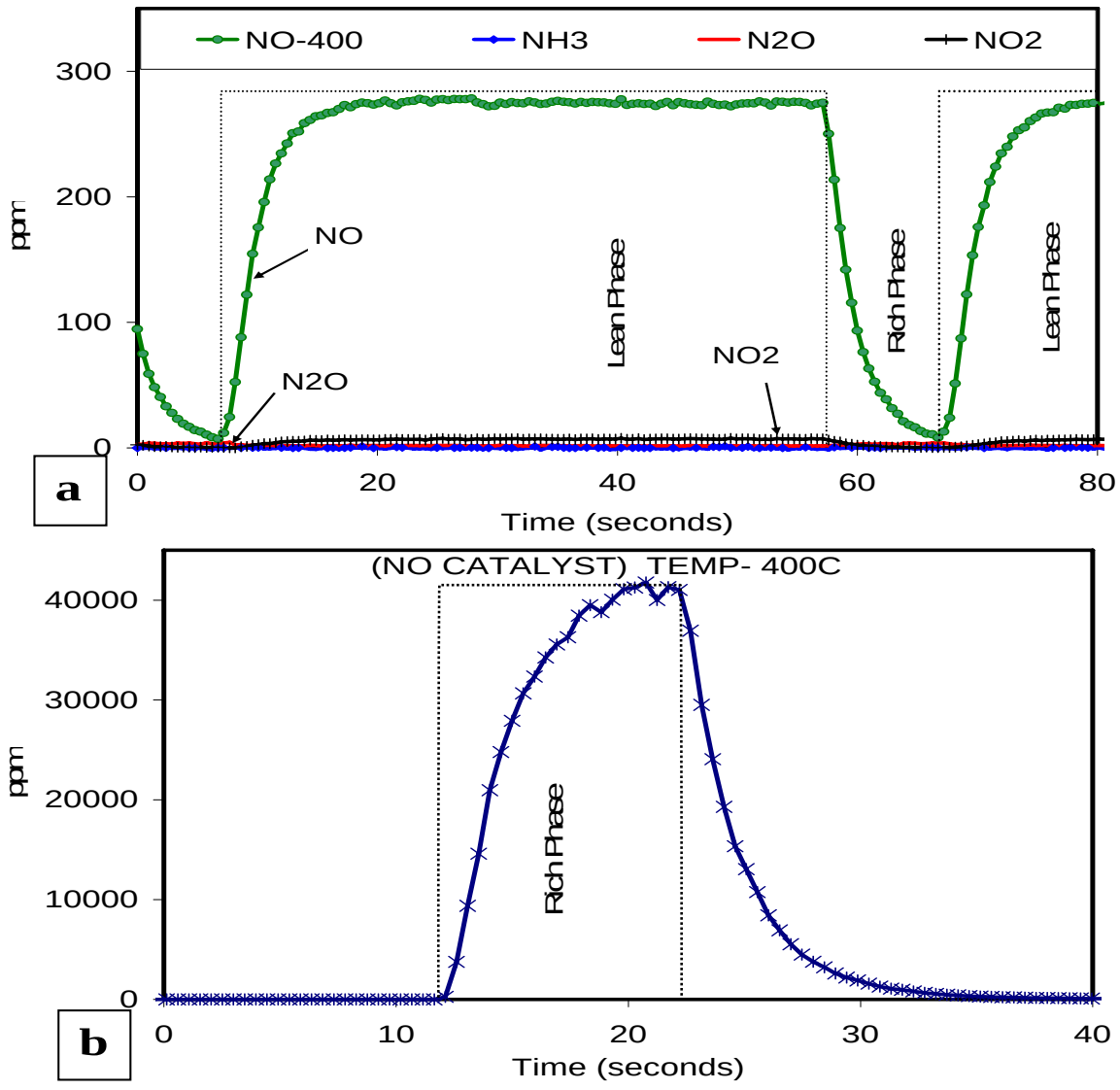

Figure 4-1: FTIR data trends for a) N species (no catalyst at 400°C), b) CO (no catalyst at 400°C)

The time for CO to reach 90% of the inlet concentration after the concentration began to change (t_{90}) was approximately 5 seconds. The same approximate t_{90} was observed when the rich phase was switched off. The time taken for NO to reach 90% of its concentration with the switch to the lean phase was approximately 6 seconds. With the switch back to a 10 second rich phase, the NO concentration did not at any instant in time go all the way to 0 ppm. These trends were observed at both test temperatures with all other conditions remaining the same. A possible reason for these observations of non-ideal behavior is that some molecules stick on the walls of the reactor during their passage, with another possibility being mixing at the gas composition transition "front" within the reactor system.

There was no NO_2 present in the reactant feed, but a very small amount, ~10 ppm, was observed in the outlet gas, which indicated that oxidation of NO on the walls of reactor occurred. The amount of N_2O observed was typically nil: however, there appeared to be a small amount of N_2O with the switch to the rich phase, indicating that some NO reacted with the walls and was reduced to N_2O in the absence of O_2. CO_2 was not observed, indicating the absence of the CO oxidation reaction with the reactor walls when CO was added. Similar trends were observed when the same experiment was conducted at 300^{o}C.

4.1.4 Summary

There was a delay in achieving the inlet concentrations observed when switching the valve between phases, likely due to mixing and some adsorption onto the reactor walls, but this was determined to be insignificant in comparison to expected changes with the catalyst present, as will be shown later in this chapter. With NO oxidation less than 5% on the walls, this impact was also determined to be insignificant and ignored. This base line experiment removes any doubts regarding significant extents of reaction occurring anywhere other than on the catalyst surface.

4.2 Experiment Set 2: Effect of O_2 in the Rich Gas Composition

4.2.1 Objective

Evaluate the effects of oxygen in the rich phase on catalyst performance and temperature.

4.2.2 Experimental Setup

Table 4-2 lists the experimental conditions used in this series of experiments.

Table 4-2: Experimental conditions to evaluate the effect of O_2 concentration in the rich phase

Flow (L/min)	14.08	**Catalyst**	Pt/ Ba/ Al_2O_3	**Sp. vel (hr^{-1})**	30,000	**Temp (^oC)**	300/400
Composition	**H_2O**	**CO_2**	**O_2**	**NO**	**CO**	**N_2**	**Time (s)**
Lean phase (%)	5	5	10	300 ppm	-	Bal	60
Rich phase (%)	5	5	0,1,2	-	4	Bal	8

4.2.3 Results & Discussion

In determining the effects of O_2 in the rich phase, the oxygen concentrations used were 0, 1 and 2%, the amount of reductant being kept constant at 4%. Furthermore, changes in catalyst performance with reaction temperature were evaluated by performing experiments at 300 and 400°C. For ease of analysis, we selected lean/rich cycle times of 60/8 seconds for discussion. The longer, 8 second, regeneration time results in easier temporal analysis. Tests were also performed with 4 and 2 second regeneration times, but the data will not be shown. The catalyst used was a $Pt/Ba/Al_2O_3$ catalyst.

4.2.3.1 Gas Composition Analysis Results

The FTIR gas analysis results show that as the O_2 was increased from 0 to 2% in the rich phase, Figure 4-2a and b, the amount of reductant exiting the catalyst decreased.

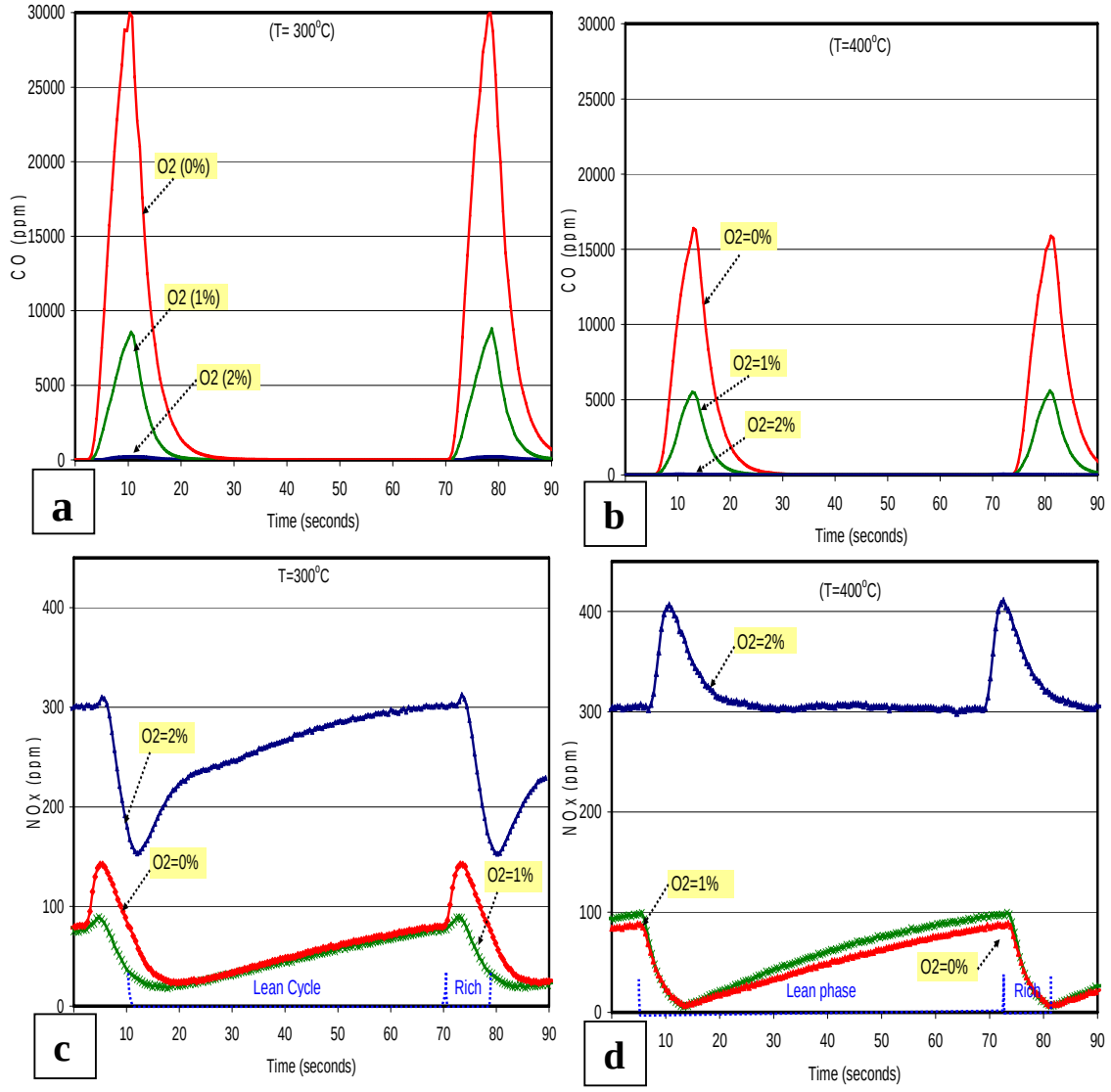

Figure 4-2: Effect of O_2 in the rich phase on a) CO at 300°C b) CO at 400°C c) NO_X species at 300°C, d) NO_X species at 400°C

No CO was observed when 2% O_2 was added, indicating that all the CO reacted on the catalyst, either with the entering O_2 or with previously trapped NO_X. One mole of CO needs 0.5 moles of O_2 for complete reaction; and this stoichiometric ratio is what was used at the extreme condition, 4% CO and 2% O_2. At both 300 and 400°C, the CO conversion increased with an increase in O_2 content of the rich phase. There is a different extent of conversion at the different temperatures. For example, the CO is consumed more efficiently with 0% O_2 at 400°C compared to 300°C, where the CO exiting was approximately 1.5% and 3.0% respectively. This is attributable to better nitrate reduction at 400°C, which is supported by the coincident smaller NO_X release observed, as seen in Figure 4-2.

NO slip would normally be expected to increase as the O_2 concentration is increased from 0 to 2%. This is due to a decrease in availability of the reductant to interact with NO_X or trapped nitrates, and therefore a build-up in nitrates would occur over several cycles. At some point a steady cycle-to-cycle conversion would be attained. Overall, if fewer nitrates were reduced in the regeneration phase, we should expect fewer available trapping sites for the subsequent lean phase. This is described by Figure 4-3.

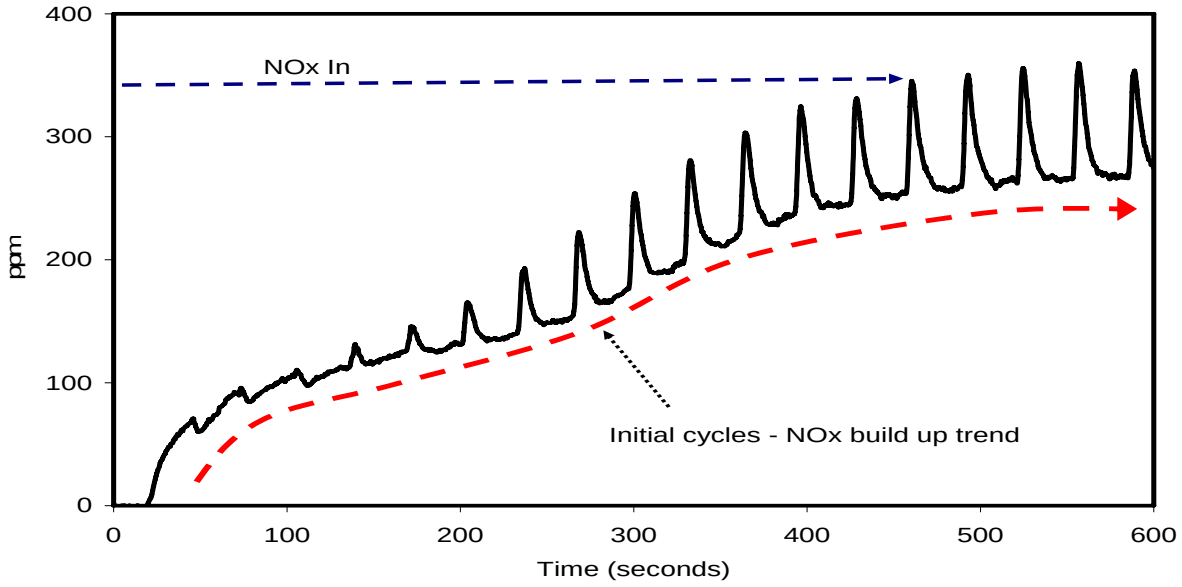

Figure 4-3: The NO_X builds up on the surface because of insufficient regeneration time during the first few cycles. Lean/rich cycle= 30/2 with 2% O_2 (rich phase).

As shown in Figure 4.2, with 0% O_2, enough reductant was available for good NO_X reduction and for surface regeneration for the next lean phase. The change in NO_X slip was small when the oxygen was increased from 0 to 1 %, as enough reductant was still present to react with NO_X species trapped on the surface during the previous lean phase. But, in increasing the O_2 from 1 to 2%, there was a significant change in the amount of NO_X trapped and released. At this high O_2 condition, the catalyst during the first few cycles becomes saturated with NO_X via nitrate formation, as there is not enough reductant available for nitrate/NO_X reduction and catalyst regeneration since the reductant is being consumed by the O_2. Therefore, after a few cycles, any NO_X entering the reactor was not trapped and simply slipped past the catalyst.

4.2.3.2 IR Camera Temperature Data Analysis

The temperature profiles along the axial direction of the catalyst monolith were analyzed in order to determine the exothermic reaction intensities on the catalyst surface during the experiments. The CO oxidation reaction is relatively easy over a Pt-based catalyst at 300 and 400°C and light-off should occur immediately. So, in any experiment where we have both CO and O_2 in the rich phase, the maximum reaction intensity is expected to be at the front of the catalyst. As the reactant CO and O_2 concentrations decrease along the catalyst axial length due to upstream reaction and consumption, so will the intensity of the reaction. The CO oxidation reaction is exothermic, so the reaction will be accompanied with a temperature rise. The largest amount of reaction occurs at the position where the highest temperature rise is observed. Along with CO oxidation, nitrate reduction is also exothermic, but less so. Due to the large differences in exothermicity, nitrate reduction could only be positively, or confidently, identified when no O_2 was added during the rich phase.

As stated above, if CO oxidation is easy, with the addition of O_2 during the rich phase, the highest temperature increase should occur at the inlet (pos-1) and a decreasing exotherm-induced temperature rise trend should be observed towards the outlet (pos-20). This is indeed the trend seen for both 300°C and 400°C as shown in Figure 4-4a and b. In all the experiments at 300 and 400°C with O_2 concentrations of 1 or 2%, the highest temperature rise was indeed observed at position 1.

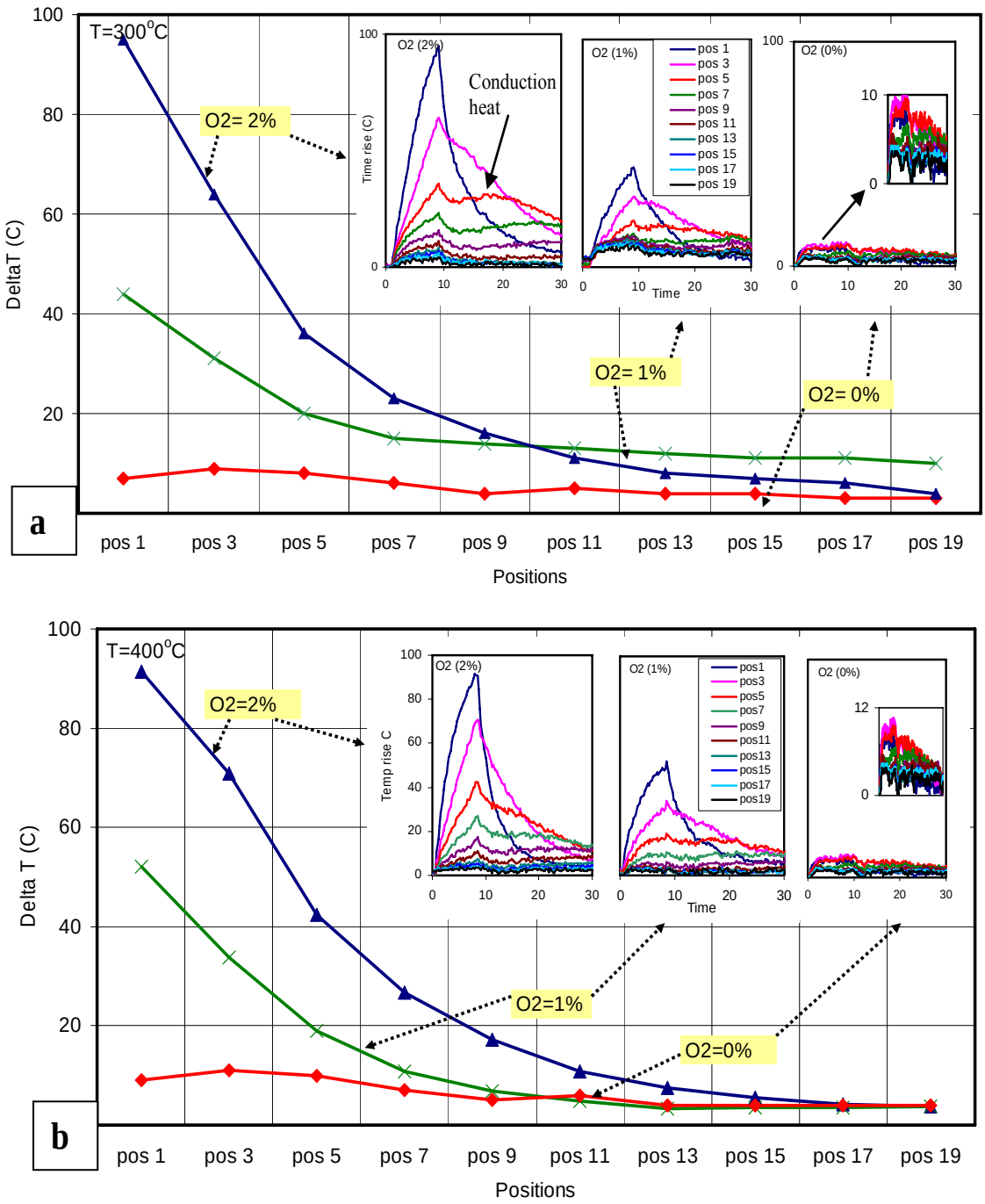

Figure 4-4: Maximum change in temperature values at different positions across the catalyst for 0, 1 and 2% O_2 & 4% CO (rich phase) at inlet catalyst temperatures of a) 300°C and b) 400°C (in inset, complete temperature profiles for each experiment)

The highest temperature rise observed was >90°C at the inlet and when CO and O_2 stoichiometric amounts were present in the rich phase i.e. 2% O_2 and 4% CO. At 1% O_2 concentration in the rich phase, there was still a large temperature rise (>40^{o}C) due to the CO oxidation reaction, plus there was residual reductant to carry out the NO_X/nitrate reduction reaction, which was not readily distinguished. But, in the experiment where there was no O_2 added in the rich phase, the only source of heat generation on the catalyst surface is from the exothermic NO_X/nitrate reduction reaction, and this accounts for the small temperature rise (<20^{o}C) observed.

With 0% oxygen, and therefore only the nitrate reduction reaction occurring, the highest temperature rise shifted from the very inlet to 15% of the axial length fraction, position 3, indicating that a maximum in NO_X/nitrate reduction occurred at that part of the catalyst. This might be due to the fact that nitrates form from NO_2. With no NO_2 available at the very inlet position, little or no nitrate forms. A build-up in NO_2 with oxidation results in nitrate formation, with NO oxidation occurring at upstream positions. The outlet position during all the experiments had the lowest temperature increase, showing that only a small amount of NO_X deposited at the downstream catalyst positions and the CO oxidation reaction was not occurring that far into the catalyst due to a lack of O_2 for reaction.

The large temperature increase with CO oxidation, >90^{o}C, at the inlet when 2% O_2 was used, also resulted in heat conduction down the catalyst, which becomes evident as a 2nd temperature increase peak at positions downstream and at later times. This heat conduction occurring on the catalyst is quite evident starting from position 5, inset Figure 4-4a. The conduction wave appeared with a delay of 10-15 seconds after switching to the rich pulse, which is several seconds after the rich phase ended. The difference in the magnitudes of the temperature rise from the reaction and that from conduction decreased down the axial length of the catalyst. This is due to less reaction intensity away from the inlet and constant loss to the gas-phase. The conduction “wave” does not result in sharp temperature rise peaks, but disperses along the catalyst length resulting in a broader temperature rise feature. Therefore, the time required for the temperature to attain the nominal starting values at the upstream axial positions was quite fast compared to the downstream/outlet positions.

4.2.4 Summary

An increase in O_2 from 0 to 2% resulted in an increase in the temperature changes observed and in less reductant availability for NO_X reduction on the catalyst at higher O_2 concentrations. More CO availability led to increased NO_X trapping along with higher overall NO reduction. Similarly, stoichiometric O_2 amounts led to small NO_X trapping and small conversion of NO_X to N_2. CO oxidation generates high temperature increases at the catalyst inlet, with nitrate reduction, although also being exothermic, showing smaller temperature changes. With 0% oxygen in the rich phase, it is simply NO_X chemistry on the surface of the catalyst that results in temperature changes, the focus of the next section.

4.3 Experiment Set 3: Different Amounts of Trapped NO_X

4.3.1 Objective

Identify the NO_X storage pattern on the catalyst surface using measurement of the heat generated during the NO_X reduction reaction.

4.3.2 Experimental Setup

Table 4-3 lists the experimental conditions used for this series of experiments.

Table 4-3: Experimental conditions to evaluate the amount of NO_X trapped

Flow (L/min)	14.08	**Catalyst**	Pt/ Ba/ Al_2O_3	**Sp. vel (hr^{-1})**	30,000	**Temp (^oC)**	300/400
Composition	**H_2O**	**CO_2**	**O_2**	**NO/NO_2**	**H_2**	**N_2**	**Time (s)**
Lean phase (%)	5	5	10	300 ppm	-	Bal	Variable
Rich phase (%)	5	5	0	-	1	Bal	Variable

4.3.3 Results & Discussion

Prior to each experiment, the catalyst was cleaned at 400°C to eliminate any residual nitrates on the surface. Therefore, all experiments were begun with a consistent surface. The same $Pt/Ba/Al_2O_3$ catalyst was used for this experiment. Also, instead of 4% CO, 1% H_2 was used during the rich phase. The reason for the smaller amount of reductant is that this will result in a longer time for the reactions to complete and therefore in more readily observable trends. Note also, H_2 is considered a better reductant for NO_X Storage/Reduction (NSR) catalysts as compared to other reductants [1,13,19]. These experiments were conducted by increasing the lean phase time from a randomly chosen minimum of 3 minutes until the time needed for catalyst saturation.

Also, tests were conducted at both 300 and 400°C, and using NO or NO_2 as the NO_X source in the lean phase. The target NO_X concentration was kept constant at 300 ppm: however, there was a small, but at least consistent, calibration error from the flow controllers. For a given target input of 300 ppm, the flow controller resulted in approximately 330 ppm of NO and 280 ppm of NO_2. For these experiment sets, the lean times used were maintained between each set and then the different amounts of NO_X deposited were calculated. The lean cycle times were 3, 5, 10, 15, 30, 60 and 120 minutes, see Figure 4-5, after which the rich phase gas composition was introduced and the temperature changes were recorded with the IR camera. The lean phase time is proportional to the amount of NO_X deposited on the surface, so by increasing the lean time more NO_X will be deposited on the surface, until saturation is reached. With increasing lean time, NO_X is *expected* to deposit from front to back; the saturation of the catalyst should start at the inlet and move towards the outlet. Both NO and NO_2 were monitored and summed to calculate total NO_X deposited. The concentration of NOx deposited in a given time interval was calculated using:

$$NO_X \text{ Accumulated (i)} = NO_X \text{ in (i)} - NO_X \text{ out (i)}$$

where (i) represent any particular time interval. So, the overall NO_X deposited for a given cycle time (complete lean phase) was calculated using:

$$\sum NO_X \text{ Accumulated} = \sum NO_X \text{ in} - \sum NO_X \text{ out}$$

The NO_X calculated from the above relation will be reported in units of cm^3 @ STP.

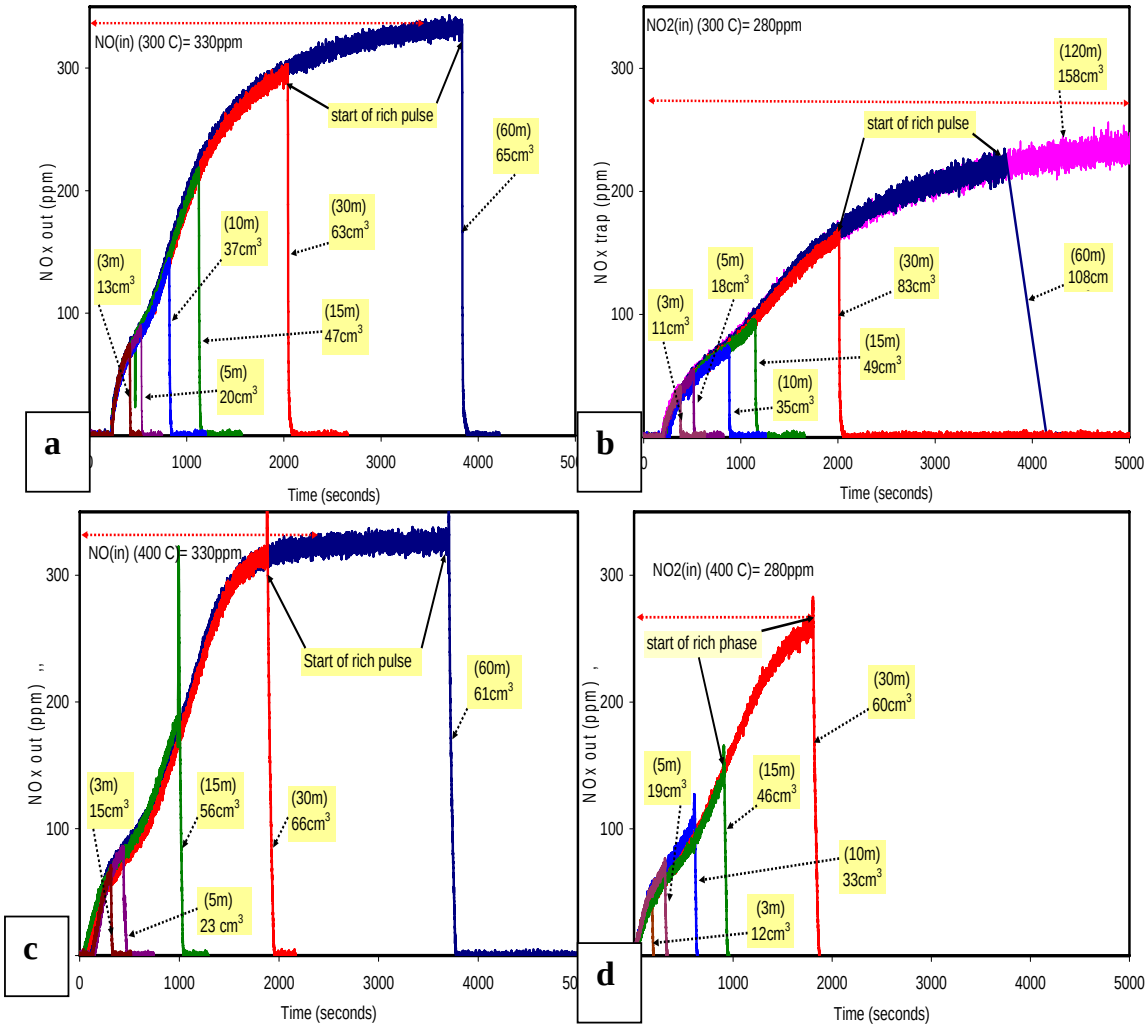

Figure 4-5: NO_X out concentrations for different lean cycle times; a) NO in at 300°C, b) NO_2 in at 300°C, c) NO in at 400°C, d) NO_2 in at 400°C

The amount of heat generated on the catalyst surface at a given point, from the temperature profiles, was calculated by integrating temperature vs. time data. Recording began just before the introduction of the rich phase and then until the temperature returned to its initial value. In order to exclude the heat associated with the conduction band in pos2-20 from the heat generated on the catalyst surface due to exothermic reduction reactions, the 2nd peak appearing at the tail end of each integrated temperature profile was removed before

calculating the amount of heat generated for each position. The sum of individual heats from all 20 positions in the run results in the total heat generated during each run. For these experiments, the intensity of the temperature change at a specific site is proportional to the amount of reaction occurring at that particular site and time on the catalyst. Table 4-1 lists the calculated NO_X deposited and the overall heat generated for each run.

Table 4-4: Calculated values of NO_X deposited and the heat generated on the catalyst

Total NO_X Deposit (STP cm^3)				
Time	**NO @ 300°C**	**NO_2 @ 300°C**	**NO @ 400°C**	**NO_2 @ 400°C**
3	13	11	15	12
5	20	18	23	19
10	37	35	36	33
15	47	49	56	46
30	63	83	66	60
60	65	108	61	
120		158		
Total Heat generated [Delta T (^oC) * Delta time (seconds)]				
Time	**NO @ 300°C**	**NO_2 @ 300°C**	**NO @ 400°C**	**NO_2 @ 400°C**
3	972	1266	232	611
5	2334	1688	1294	1085
10	4746	4617	4373	3209
15	7617	8867	5336	3941
30	8729	13149	6784	9935
60	14354	18183	6939	
120		24927		

The amounts of NO_X deposited and the total amounts of heat generated (integrated temperature increase over time) for each run, for different lean phase times as graphically summarized in Figure 4-6.

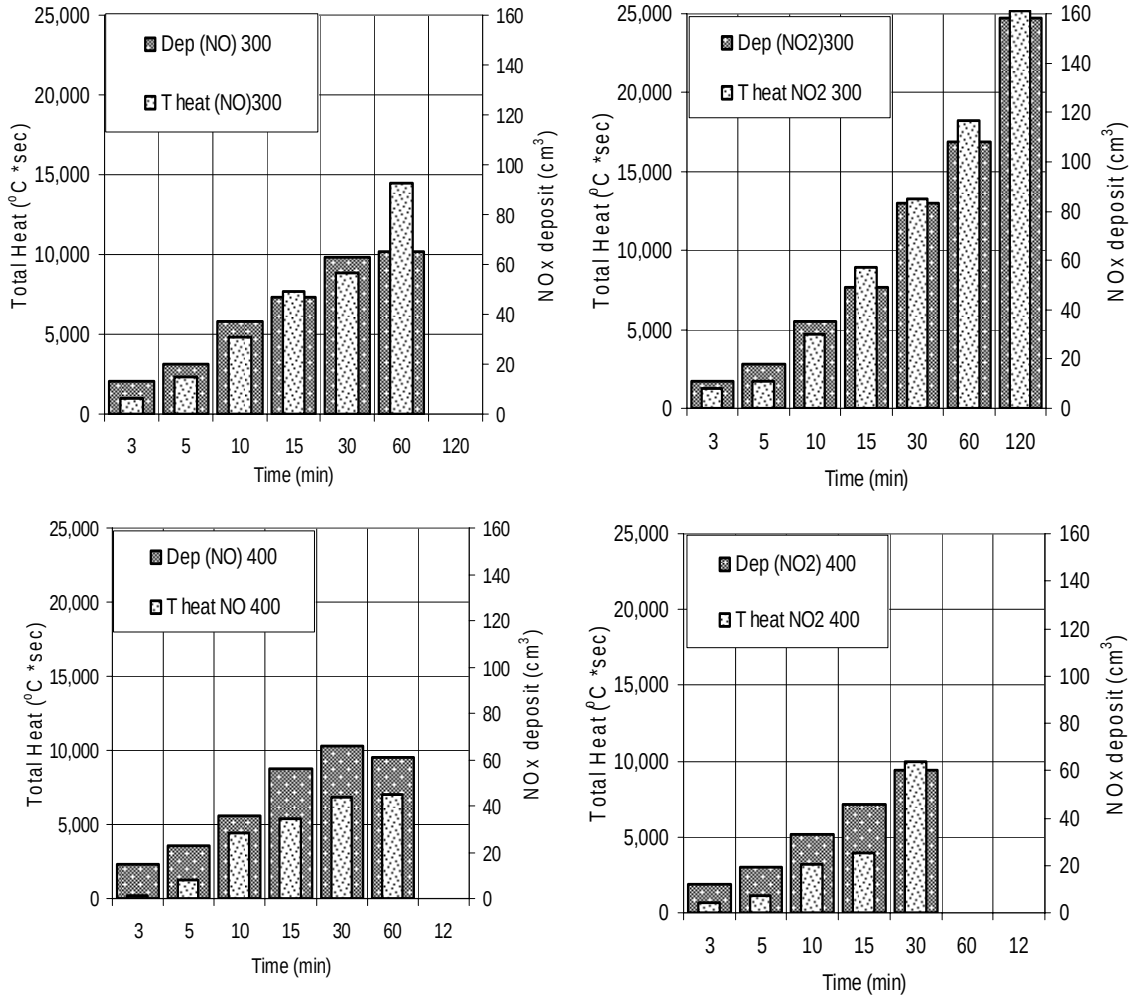

Figure 4-6: Relationship between the NO_X deposited (cm^3 at STP) and amount of Heat generated (Delta Temp/ Delta time)

To more clearly demonstrate the relationship between the different variables tested and the factors that affect the NO_X deposited on the catalyst surface, our discussion is divided into 2 sections. The first section describes the effects of using NO or NO_2 in our feed stream at 300 and 400°C. The second section focuses on the effects of temperature, 300 and 400°C, on the

formation of nitrates from NO or NO_2 in the feed. Although these are indeed the same experiments, the discussion focuses on the separate effects and presents a clearer description of the effects.

4.3.3.1 The Effects of Using NO or NO_2 in the Feed

4.3.3.1.1 Temperature = 300°C

Differences in the amount of NO_X trapped were observed when using NO_2 as compared to NO in the feed, as shown in Figure 4.7a and b. The amount of NO_X trapped at complete saturation on the same catalyst when testing at 300°C increased from 65 cm^3 with NO to 158 cm^3 with NO_2. This result is consistent with past studies [1,2,10,41] that showed increased nitrate formation rates and coverage's when using NO_2. An extra 60 minutes of exposure to NO_2 was needed to achieve catalyst saturation as compared to using NO, clearly showing that extra storage sites were being occupied with NO_2 as the NO_X source.

The total heat generated and NO_X deposited values were similar when using either NO or NO_2 in the feed for short NO_X adsorption times, but deviated significantly once the catalyst started to approach saturation. The total amount deposited when NO was input was 41% and 57% less for the amount of NO_X deposited and the heat generated respectively at the end of the full saturation runs as compared to when NO_2 was used. The slower/decreased NO_X trapping and nitrate formation with NO can be partly attributed to the need for the NO oxidation reaction, as NO_2 is considered a nitrate precursor. Another reason for the larger amount of NO_X deposited when using NO_2, is that NO_2 can also act as an oxygen source for nitrate formation. The three major reactions involved in nitrate formation [10] are:

$BaO + 2NO + 3O^* \rightarrow Ba(NO_3)_2$ in case of NO in feed

$BaO + 2NO_2 + O^* \rightarrow Ba(NO_3)_2$ in case of NO_2 in feed

$BaO + 3NO_2 \rightarrow Ba(NO_3)_2 + NO$

As shown, the first two result in nitrate formation-using O*, which originates from O_2. The third reaction can only occur with NO_2. It has been proposed [10] that disproportionation is a dominant nitrate formation mechanism at sites not near Pt, where O* would be formed. Therefore in experiments where NO_2 is input instead of NO, the rate of $Ba(NO_3)_2$ formation

will be higher, as the disproportionation reaction at sites not near Pt can account for further formation of Ba nitrates.

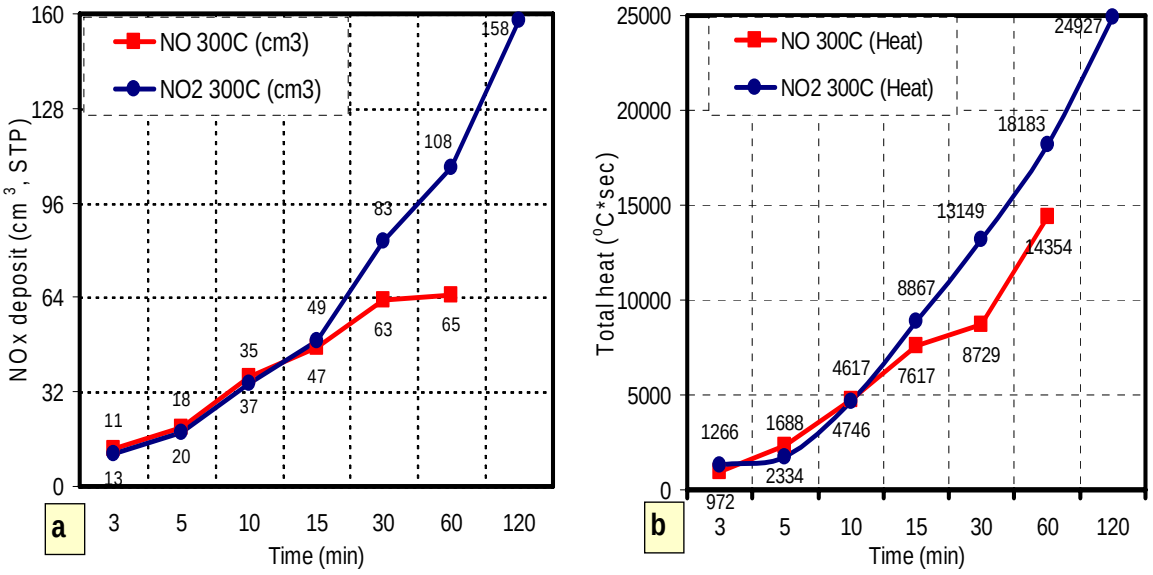

Figure 4-7: Comparison of NO and NO_2 behavior at 300°C; a) NO_X deposit, b) total heat generated

During regeneration, the heat released and temperature rise represent the amount of NO_X that was deposited on the surface at that site, assuming that the surface species are identical. The spatially resolved amounts of heat generated and total NO_X deposited were therefore compared to understand where the NO_X was deposited on the catalyst. To do this, the total heat generated for each run, which is the sum of heat generated along the axial direction of the catalyst, was divided into axial components across the catalyst surface to understand the deposition pattern, see Figure 4-8.

Each point represents the amount of heat generated locally, chosen for these experiments as 20 equidistant positions (pos) along the radially-central, axial direction of the catalyst. For the smaller time intervals, the axial patterns in amount of NO_X deposited were similar. Nitrate reduction occurred at the upstream positions, indicating that NO_X was trapped towards the inlet of the sample. The heat generation value at position 1 when NO_2 was used,

which correlates to the NO_X deposited at the very inlet position, increases with increasing lean cycle times, demonstrating an increased sorption at the very inlet position. However, with increasing trapping time, the inlet positions showed smaller increases in NO_X adsorption, as compared to downstream positions.

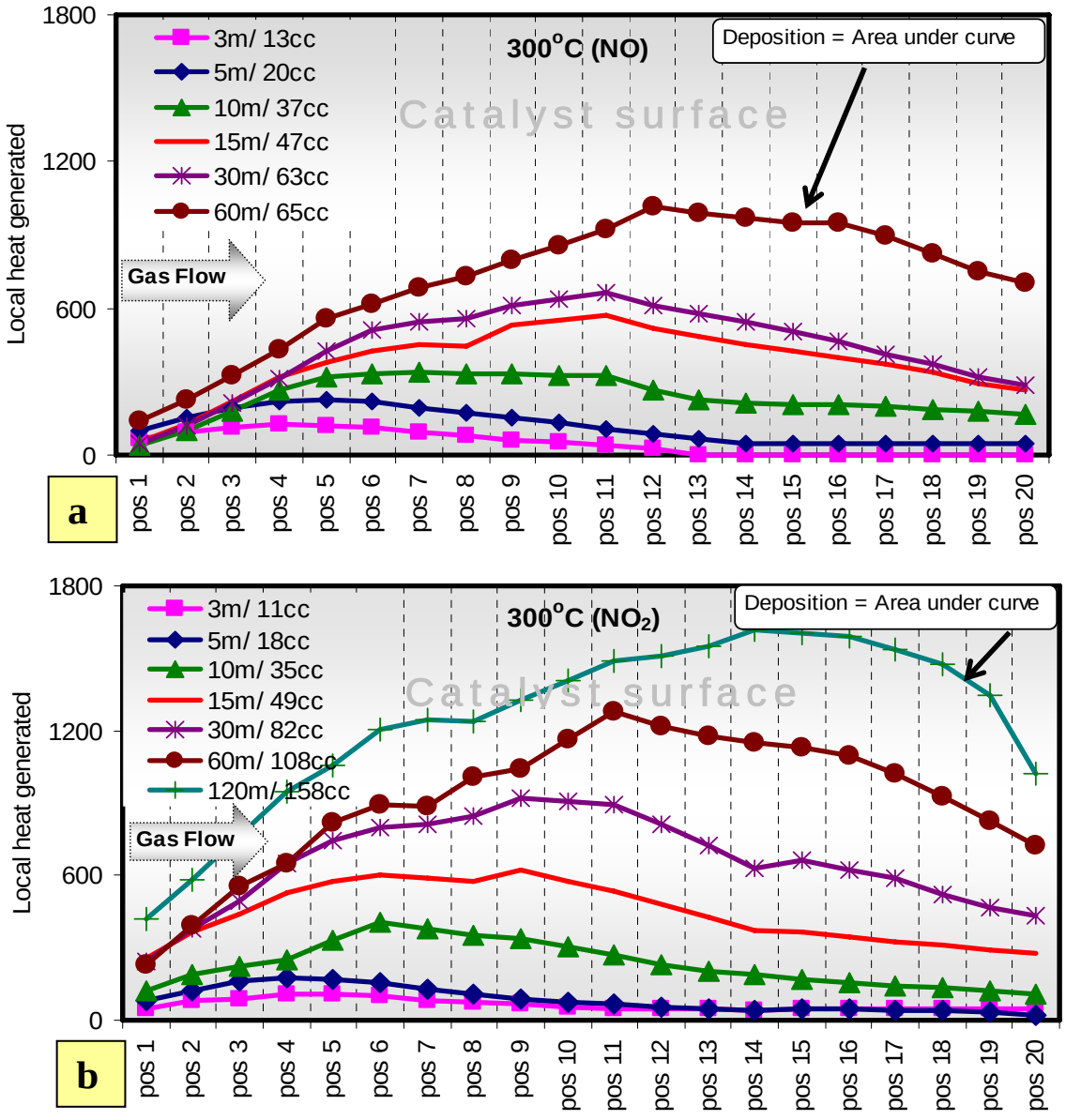

Figure 4-8: Local heat generated at each position across catalyst for tests at 300°C using a) NO and b) NO_2

In the case of NO_2, the inlet sites showed more storage capacity than in the case of NO as see by comparing Figure 4-8 a and b. The deposition at the inlet positions when NO was used seems to be restricted, possibly due to the fact that at those sites NO oxidation was occurring and not enough NO_2 was present to drive the reaction for nitrate formation. Furthermore, even though with NO_2 as the NO_X source there was no NO oxidation constraint at the initial positions, the overall deposition trend still matched the trend when NO was used as the NO_X source in the feed; increasing amounts deposited downstream relative to the amount deposited at the very inlet.

As mentioned above, it was expected that trapping would move from front to back along the catalyst. With NO as the source, an absence of NO_2 might shift this pattern to show maximum storage at slightly downstream positions where enough NO_2 is present via NO oxidation. But with NO_2 there should be no such constraint. At this stage, with the data obtained it is difficult to give a conclusive answer as to why the IR thermography data indicate that NO_2 did not simply saturate from front to back, but several possibilities that could cause this behavior will be discussed.

One possible reason is that at 300^oC it is still difficult to fully regenerate the catalyst, or remove all the NO_X species during the rich phase. Regeneration improvement, i.e., more nitrate reduction, could occur at the downstream positions because of some temperature increase from conduction from the exotherms generated by the reactions upstream. This poor release trend of NO_X species from the surface at 300^oC compared to higher temperatures has also been shown in previous work by Balcon et al. [43], who studied the release rate of NO_X as a function of both temperature and gas composition.

Another possible reason for this reduced storage at the catalyst inlet sites is the fact that NO and NO_2 exposure results in both nitrite and nitrate formation. Previous work [44] has demonstrated a thermal stability difference between the two species with respect to temperature, with an increase in heating from 300^oC to 400^oC causing a complete desorption of all nitrates and nitrites. Another study [45] also demonstrated that it is the nitrates that are the most abundant species at 350^oC, but at lower temperatures some nitrites did exist and are proposed to form first and then become oxidized to nitrates. Nitrite reduction is less

exothermic than nitrate reduction and therefore could lead to less heat generated and account for the observed trend i.e. nitrites are formed at upstream positions and more nitrates at downstream positions. Lastly, the Pt and Ba distribution on the catalyst surface may be non-uniform on a large scale. This seems less likely, but needs future confirmation.

4.3.3.1.2 Temperature = 400°C

The calculated NO_X storage capacity trends using either NO or NO_2 were not very different. As shown in Figure 4-9, the saturated catalyst contains approximately same amount of NO_X with either NO or NO_2, 60 cm^3. Also, at 400°C with NO in the feed, the results from the 30 and 60 minute experiments were similar, since the catalyst was saturated after 30 minutes.

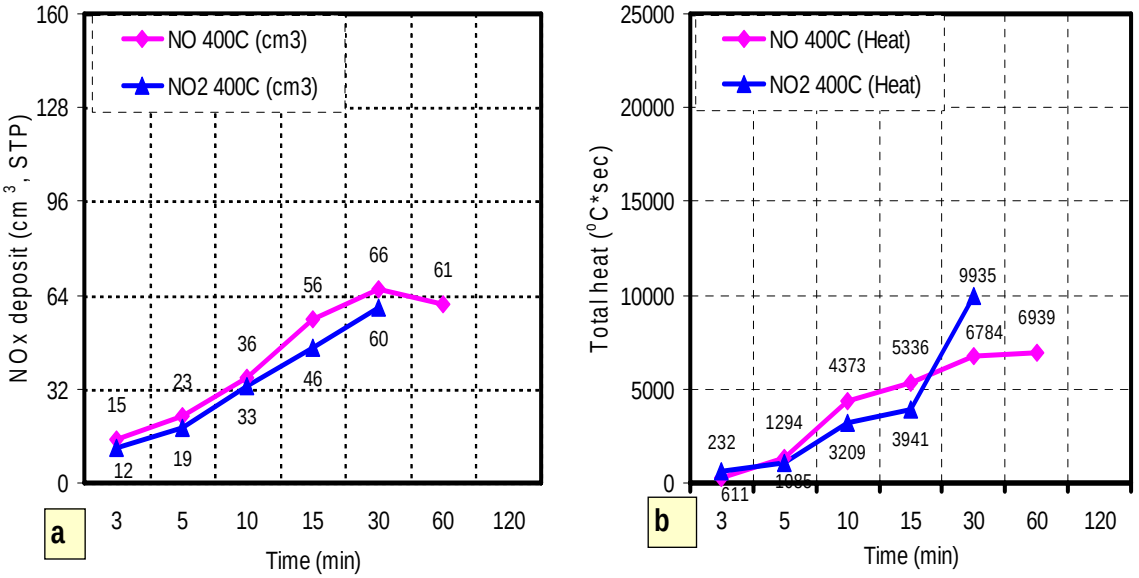

Figure 4-9: Comparison of NO and NO_2 trapping behavior at 400°C a) NO_X deposit, b) total heat

With 400°C operation, the location of the sorbed NO_X is more evenly distributed across the surface, especially in the experiment where saturation was reached when NO_2 was used, see Figure 4-10b. This is different than the data collected at 300°C, where an observed build-up from the inlet toward downstream positions formed, but matches the preconceived notion of

axial build-up from inlet to outlet with NO_2. With NO as the inlet NO_X source, Figure 4-10a, the most inlet positions (pos1-5) sorbed less than sites just downstream. The reason, as discussed earlier, is related to the initial sites not being exposed to the higher NO_2 concentrations, due to NO oxidation limitations.

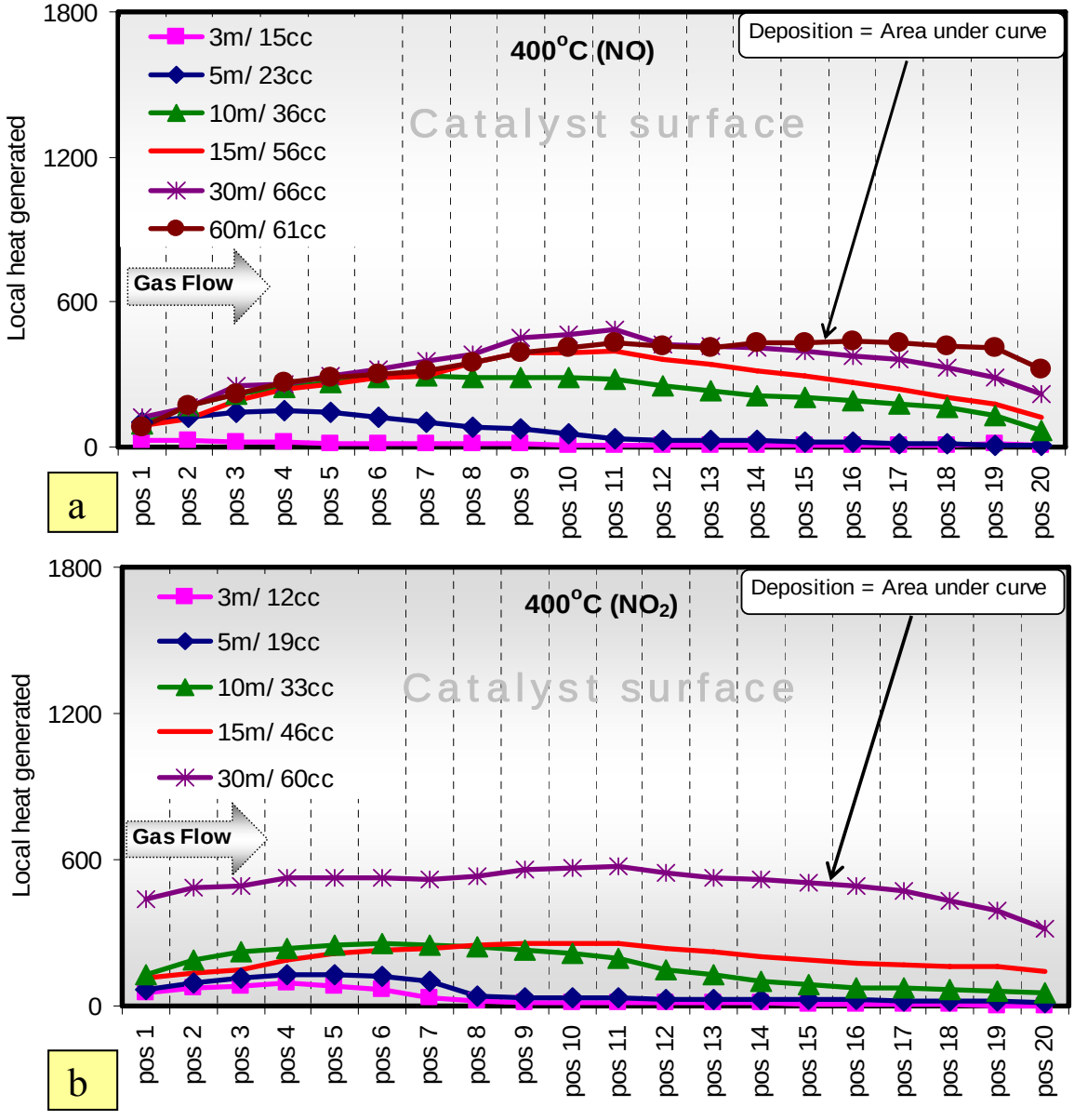

Figure 4-10: Local heat generated at each position along the axial length of the catalyst at 400°C using a) NO and b) NO_2

Even though the saturation NO_X amount (calculated) is same approx 60 cm^3 in both cases (NO and NO_2), comparing the heat generation at inlet positions for saturation runs showed a difference in the distribution of NO_X along the catalyst for these two runs. The heat generated data obtained at 400^oC for the saturation run indicates more NO_X was trapped compared to the calculated amount of NO_X via gas analysis, especially at the outlet positions of the catalyst i.e. after pos 14, with an increase in lean time from 30 to 60 min. The reason for this discrepancy is not fully known.

4.3.3.2 The Effect of Temperature

The data to be discussed below have already been shown above, but in some cases will be pictorially re-presented for clarity.

4.3.3.2.1 NO in Feed

As shown in Figure 4-11, with NO as the NO_X source, similar amounts are trapped at both test temperatures with each time interval. For example, for the saturation run, only a small difference, about 4cm^3, in the amount of NO_X trapped was observed when comparing operation at 300 and 400°C. However, the heat generated data indicate that there is a difference between 300 and 400°C, once the catalyst was saturated. Much smaller differences were observed at shorter lean phase times.

Assuming that the heat generated data is representative, this decreasing difference with shorter lean-phase times can be accounted for by recognizing that at shorter storage times there is an independence of storage on temperature due the abundant availability of sites [46]. At longer lean phase times, the effects of temperature on nitrate stability become more apparent. Another study, by Koltsakis et. al. [33] focused on understanding NO_X release at the beginning of regeneration phase and showed that the NO release trends for 300 and 400^oC were very similar for short sorption times but showed considerable difference at these same temperatures for longer lean phase times. Such a trend matches the results in Figure 4-11b, where there was a difference in heat generated at saturation. Although similar amounts were trapped, different amounts of NO_X were released, but unconverted to N_2, i.e. differences in conversion were obtained during the rich phase. Some other factors which might result in

the different heat generated patterns include the following. The difference in heat generated could be due to different NO_X species, i.e. nitrates and nitrites, on the catalyst surface. Since their reduction reactions have different exothermic extents, different levels of heat on the surface would be generated. This difference is present even in small lean cycles but gets more evident as more and more NO_X is deposited on the catalyst surface.

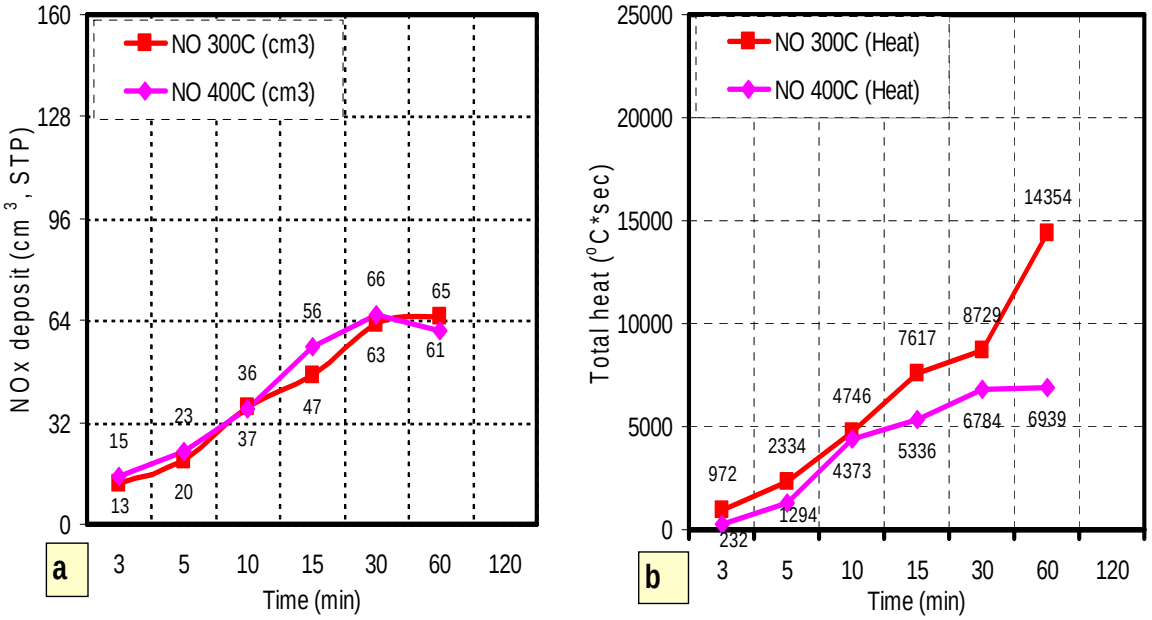

Figure 4-11: Comparison of NO in at 300°C and 400°C on a) NO_X deposit, b) total heat

Another possibility is that trapping can occur at different catalyst sites at these different temperatures. For example, sites close to Pt may result in different heats released, or a different reduction extent, than sites further from Pt. Even the surface emissivity, which strongly depends on the surface temperature, might have influenced the temperature data recorded by the IR camera. All these reasons need further study to verify the cause of the difference, which is beyond the scope of this work.

Again, the IR camera data was spatially (axially) evaluated to generate temperature profiles of the catalyst surface during regeneration. As shown in Figure 4-12, the inlet positions during each run again showed a limited amount of NO_X trapped on the surface when NO was

used, at both 300 and 400°C. At the other extreme, for the catalyst saturation run, the heat generated during regeneration is distributed more evenly across the catalyst with maximum deposition appearing not at the inlet positions, but downstream with maxima appearing towards the middle of the catalyst.

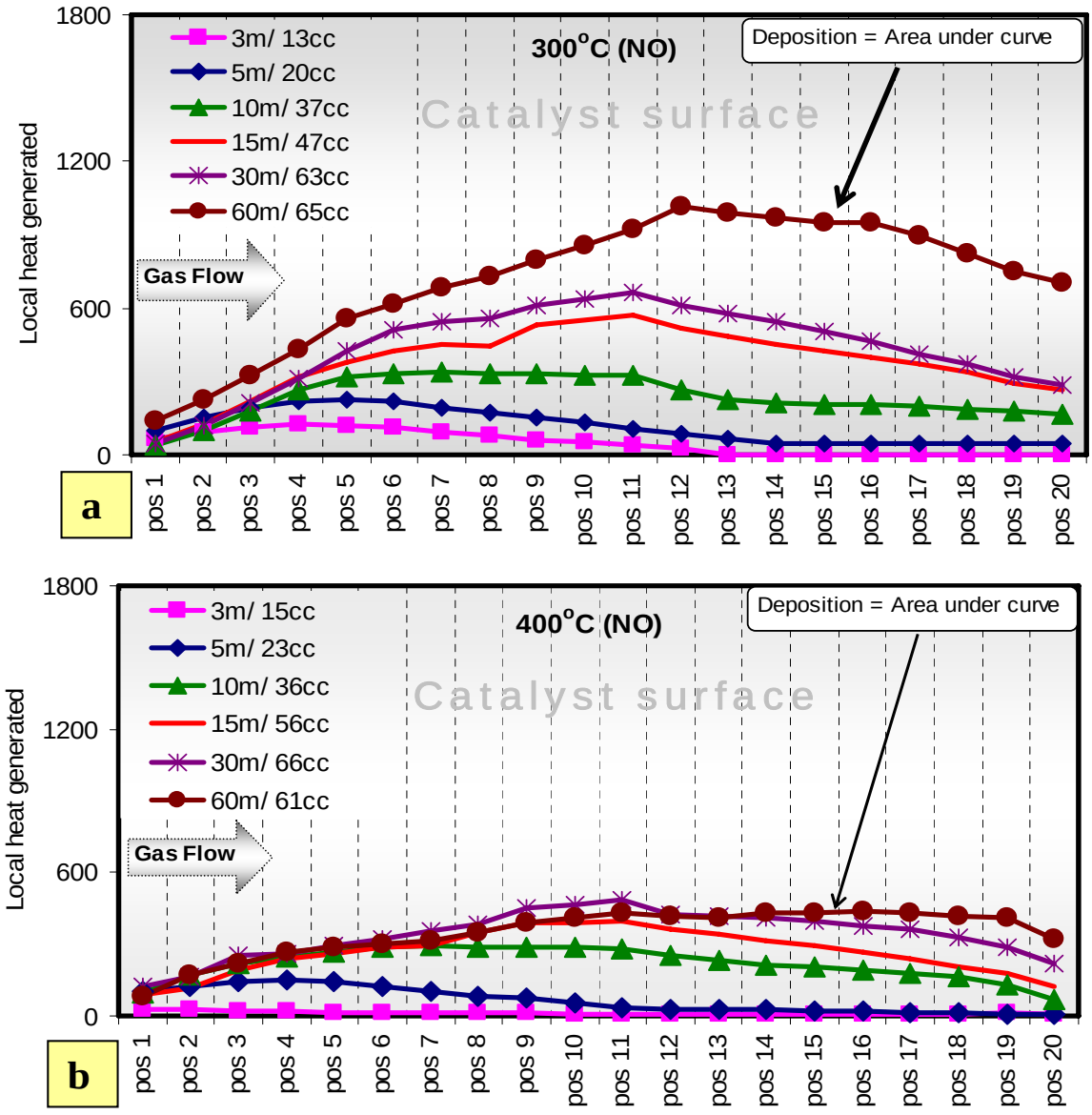

Figure 4-12: Heat generated at each position across the catalyst surface with NO in the feed at a) 300°C and b) 400°C

4.3.3.2.2 NO_2 in Feed

With NO_2 in the feed stream, Figure 4-13, an effect of temperature is clearly observed. The increase in operating temperature resulted in a 98 cm^3 decrease in the amount of NO_X trapped at saturation on the surface during the lean phase. The same trend was observed from the IR thermography data. The decrease in amount trapped with increasing temperature is due to decreased nitrate stability with increasing temperature.

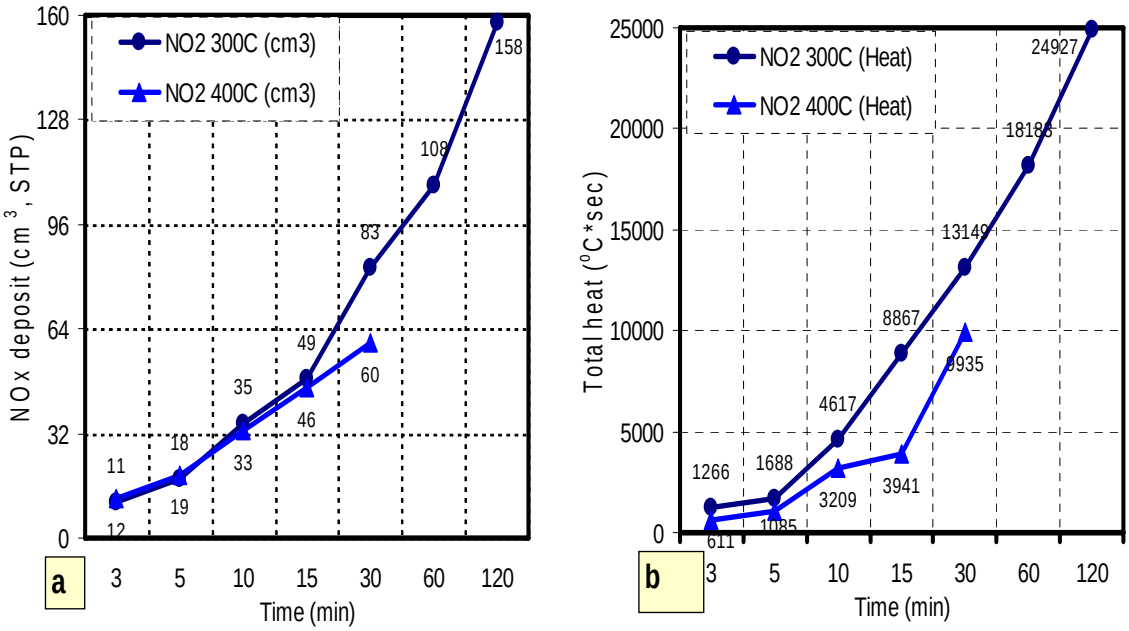

Figure 4-13: Comparison of NO_2 in at 300 and 400°C on a) NO_X deposit and b) total heat

As mentioned, at 400°C, although the sorption capacity of the catalyst is reduced compared to 300°C, the NO_2 precursor had no difficulty in causing the occupation of the inlet/upstream catalyst positions as shown in Figure 4-14b. At saturation, there is little to no axial gradient in NO_X trapped along the catalyst with 400°C operation. The overall trapping trends at 300°C were similar those noted previously where an increase in the lean phase time resulted in a systematic coverage of the catalyst surface from inlet towards outlet positions.

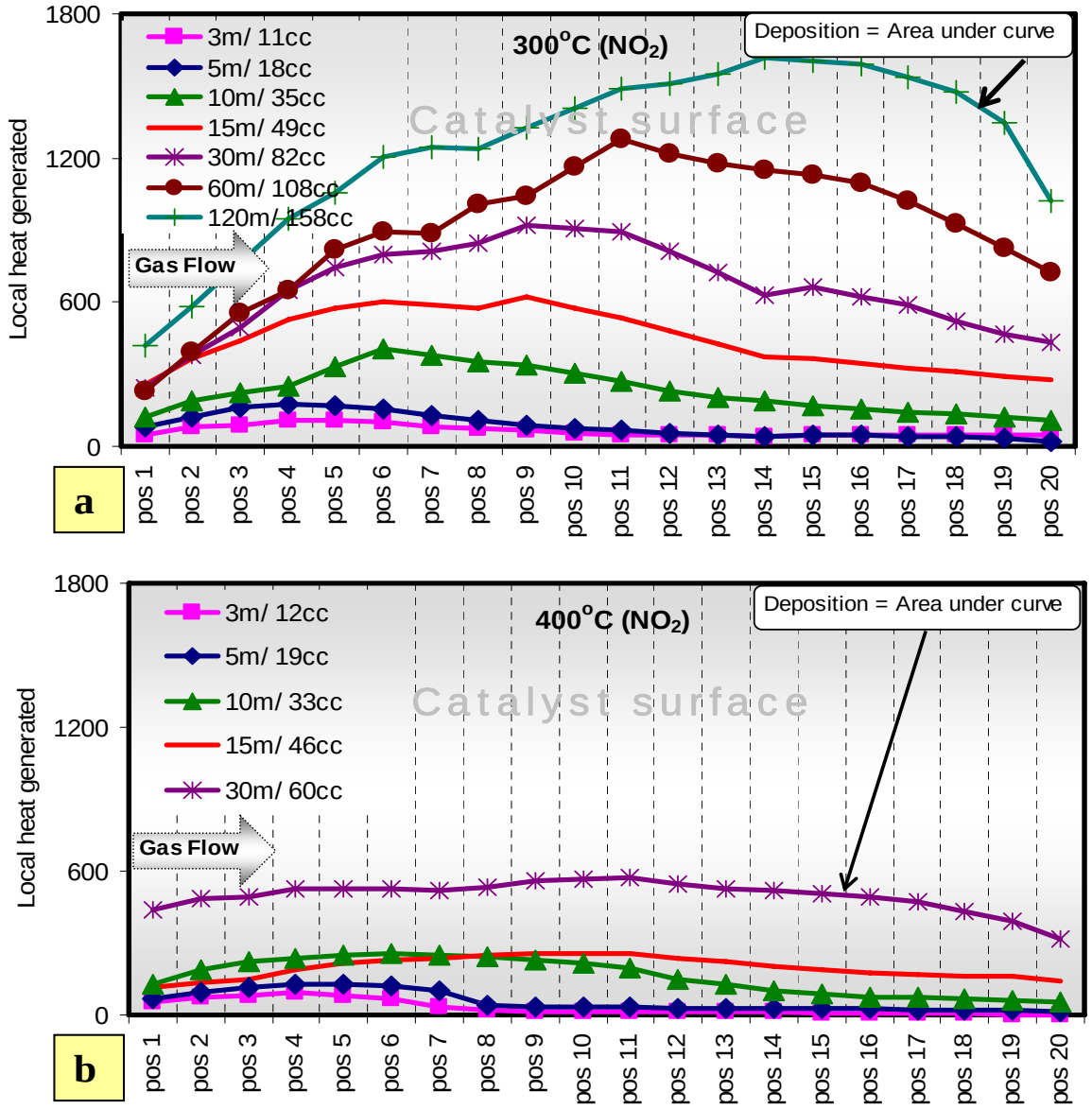

Figure 4-14: Heat generated at each position across the catalyst with NO_2 in at reactor inlet temperatures of a) 300°C and b) 400°C

4.3.4 Summary

With the third set of experiments, the objective to understand the axial deposition of NO_X on the catalyst surface was achieved. The data also indicate that previously unresolved chemistry is occurring on the catalyst surface with the introduction of the rich gas.

Chapter 5: Conclusions

This project addressed the effects of temperature, rich phase oxygen addition and NO or NO_2 use as a source of NO_X on NSR catalyst performance and chemistry. Also, the gradients in NO_X trapping on the catalyst were also characterized. A focus of the work was the use of IR thermography as a device to measure these effects and their distribution across the catalyst surface.

Specifically, a high resolution IR camera was tested and found to be accurate in evaluating temperature distributions as a function of time and position on a diesel NO_X adsorber catalyst. The exothermic nitrate reduction reaction was successfully used to determine the amount of NO_X deposited on the surface at different locations.

The other results obtained from these studies are:

- With the addition of O_2 during the rich phase, the temperature on the catalyst rose due to the exothermic CO + O_2 oxidation reaction. The highest temperature rise observed was ~100^oC with 2% O_2 and 4% CO, which was measured at the very inlet of the sample. Since the highest temperature peaks were at very front of the catalyst, this demonstrated CO oxidation is easy under these test conditions. The catalyst outlet positions in all experiments showed the least temperature rise indicating less availability of reductant and O_2 or less NO_X was deposited at the downstream locations.
- With standard cycling experiments, using 60 seconds for lean and 8 seconds for rich, the highest temperature measured occurred at position 3 when no O_2 was added to the rich-phase gas mixture. This was attributed to the need for NO oxidation in the first few positions, with the NO_2 product being the intermediate for storage.
- The measured heat generated during regeneration was consistent with the calculated amount of NO_X trapped.
- As the lean phase time increased, the calculated NO_X accumulated increased and the axial saturation pattern moved from the front of the catalyst towards the back of the catalyst, except when NO_2 was used as the NO_X source at 400°C.

- Increasing the temperature from 300 to 400°C resulted in a decrease in the amount of NO_X trapped due to a decrease in nitrate stability.
- There was a clear improvement in NO_X trapping when using NO_2 instead of NO in the feed.

Finally, the study showed the significance of using IR thermography as a tool to obtain very clear temperature gradients on catalysts and axial NO_X concentration profiles on NO_X adsorber catalysts during stimulated operation. A graphical summary of the distribution results is shown in Figure 5.1.

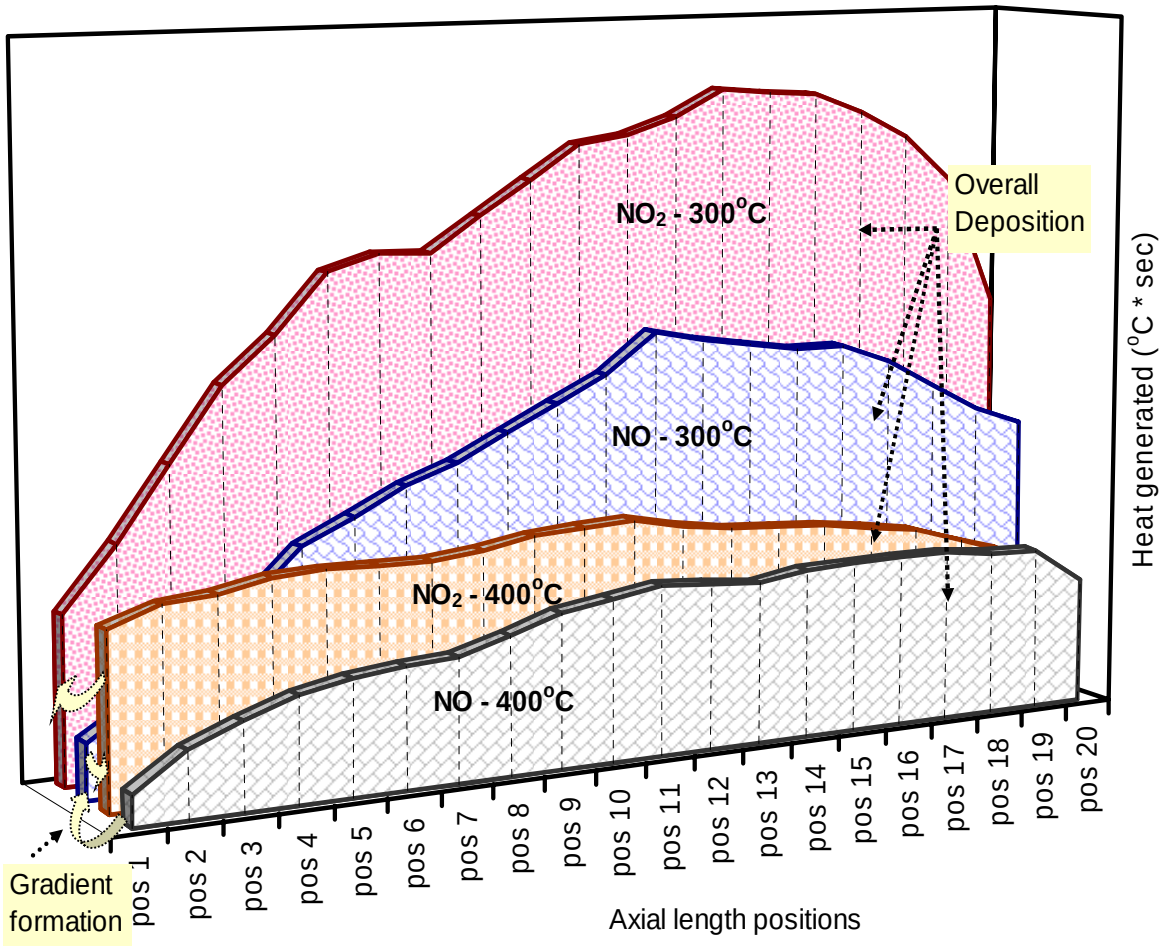

Figure 5-1: Amount of NO_X stored in each section of the catalyst

The IR thermography technique allows measurement of temperature changes occurring on a catalyst surface. Extrapolating we can say that using this technique:

- provides more descriptive data for model development;
- can help minimize catalyst volume;
- can be used to design catalysts; and
- can monitor axial gradients in poisoning and thermal degradation.

Chapter 6: Recommendations

Control of exhaust emissions from diesel engines is at a relatively early stage of development, progress is rapid and exciting, and new results may be expected in the near future. Future work related to this thesis is directed at the application of IR thermography and answering some remaining questions that were not resolved in this work, but could add to the conclusions drawn.

- First, the distribution of Pt/Ba on the catalyst should be investigated by means of XRD or some other technique.
- To further verify axial gradients, the catalyst itself could be incrementally sliced by removing a section from the inlet and adjusting the space velocity in order to keep the relative flow consistent. This would make the comparison between the gradients formed on the two different lengths of catalyst surface easy while ruling out the role played by distributions of the catalyst components on the surface.
- To validate one proposed explanation for the 300^{o}C experiments, regarding low temperature regeneration not proving effective resulting in residual NO_X on the surface, an experiment could be performed where we introduce either a high reductant amount or take the system to elevated temperatures once the rich phase is stopped. Any "extra" release can then be observed via IR thermography or gas analysis especially at the inlet positions.
- Evaluating axial gradients at other temperatures, e.g. 250, 350, and 450°C, can further characterize the sorption and regeneration trends.
- An experiment with a combination of different NO and NO_2 ratios can further help to model a system with best performance and the desired composition can be attained by making changes in diesel oxidation catalyst upstream in the exhaust.
- For long run experiments at high temperature where catalyst degradation is suspected the camera should be zero checked for true emissivity values.

References

[1] William S. Epling, Larry E. Campbell, Aleksey Yezerets, Neal W. Currier. *Overview of the Fundamental Reactions and Degradation Mechanisms of NO_X Storage/Reduction Catalysts*. Catalysis Reviews, Volume 46, Issue2, December 2004, pages 163 – 245.

[2] Louise Olsson, Westerberg, B. Hans Persson, Erik Fridell, Magnus Skoglundh, and Bengt Andersson. *A Kinetic Study of Oxygen Adsorption/Desorption and NO Oxidation over Pt/Al_2O_3 Catalysts*. J. Phys. Chem. B 1999, 103, 10433-10439.

[3] Sophie Salasc, Magnus Skoglundh and Erik Fridell. *A comparison between Pt and Pd in NO_X storage catalysts.* Applied Catalysis B: Environmental Catalysis B: Environmental Volume 36, Issue 2, 20 February 2002, Pages 145-160.

[4] Annika Amberntsson, Erik Fridell and Magnus Skoglundh. *Influence of platinum and rhodium composition on the NO_X storage and sulphur tolerance of a barium based NO_X storage catalyst.* Applied Catalysis B: Environmental, Volume 46, Issue 3, 28 November 2003, Pages 429-439.

[5] Louise Olsson and Erik Fridell. *The Influence of Pt Oxide Formation and Pt Dispersion on the Reactions $NO_2 \Leftrightarrow NO+1/2\ O_2$ over Pt/Al_2O_3 and $Pt/BaO/Al_2O_3$*.Journal of Catalysis, Volume 210, Issue2, 10 September 2002, Pages 340-353.

[6] S.S. Mullaa, N. Chena, W.N. Delgassa, W.S. Epling and F.H. Ribeiroa. *NO_2 inhibits the catalytic reaction of NO and O_2 over Pt.* Catalysis Letters Vol. 100, Nos. 3–4, April 05- 267.

[7] J. Segner, W. Vielhaber and G. Ertl, Isr. J. Chem. 22 (1982) 375. Citation.

[8] Fridell, E., Skoglundh, M., Westerberg, B., Johansson, S. and Smedler, G. *NO_X Storage in Barium-Containing Catalysts*. (1999) J. Catal. 183, p. 196.

[9] Todd J. Toops, D.B.Smith, W.P. Partridge, W.S. Epling. *NO_X Adsorption on $Pt/K/Al_2O_3$ and the quantitative effects of H_2O and CO_2* – Proceedings of the Third Joint Meeting of the U.S. Sections of the Combustion Institute.

[10] H. Mahzoul, J. F. Brilhac and P. Gilot. *Experimental and mechanistic study of NO_X adsorption over NO_X trap catalysts.* Applied Catalysis B: Environmental Volume 20, Issue 1, 4 January 1999, Pages 47-55.

[11] Lietti, L., Forzatti, P. Nova, I. and Tronconi, E. (2001) J. Catal. 204, p. 175.

[12] Theis, J. Li, J. Ura, J. and Hurley, R. SAE Technical Paper Series 2002-01-0733.

[13] Abdulhamid, H., Fridell, E. and Skoglundh, M. *Influence of the type of reducing agent (H_2, CO, C_3H_6 and C_3H_8) on the reduction of stored NO_X in a Pt/BaO/Al_2O_3 model catalyst* . (2004) Topics Catal. 30/31, p. 161.

[14] I.V.Yentekakis, M. Konsolakis, R.M. Lambert, N. Macleod, L. Nalbantian. *Extraordinarily effective promotion by sodium in emission control catalysis: NO reduction by propene over Na-promoted Pt/g-Al_2O_3-* Applied Catalysis B: Environmental 22 (1999) 123–133.

[15] Burch, J. P. Breen and F. C. Meunier. *A review of the selective reduction of NO_X with hydrocarbons under lean-burn conditions with non-zeolitic oxide and platinum group metal catalysts.* Applied Catalysis B: Environmental Volume 39, Issue 4, 20 December 2002, Pages 283-303.

[16] Akira Obuchi, Akihik Ohi, Masato Nakamura, Atsushi Ogata, Koichi Mizuno and Hideo Ohuchi. *Performance of platinum-group metal catalysts for the selective reduction of nitrogen oxides by hydrocarbons*. Applied Catalysis B: Environmental Volume 2, Issue 1, 15 March 1993, Pages 71-80.

[17] David James, Elodie Fourre, Masaru Ishii and Michael Bowker. *Catalytic decomposition/regeneration of Pt/Ba(NO_3)$_2$ catalysts: NO_X storage and reduction.* Applied Catalysis B: Environmental Volume 45, Issue 2, 30 September 2003, Pages 147-159.

[18] T. Okuhara, Y. Hasada and M. Misono. *In situ diffuse reflectance IR of catalytic reduction of nitrogen oxides by propene in the presence of oxygen over silica-supported platinum.* Catalysis Today 35 (1997) 83-88.

[19] Mahzoul, H., Gilot, P., Brilhac, J.F. & Stanmore, B. *Reduction of NO_X over a NO_X trap catalyst and the regeneration behavior of adsorbed SO_2.* (2001) Topics Catal. 16/17, p. 293.

[20] Fang, H., Wang, J., Yu, R., Wan, C. and Howden, K. SAE Technical Paper Series 2002-01-2889.

[21] R. Burch, P.J. Millington, A.P Walkerb. *Mechanism of the selective reduction of nitrogen monoxide on platinum-based catalysts in the presence of excess oxygen.* Applied Catalysis B environmental, vol 4 (1994) 65-94.

[22] Brian West, Shean Huff, James Parks, Sam Lewis, Jae-Soon Choi, William Partridge and John Storey. *Assessing reductant chemistry during in-cylinder regeneration of diesel Lean NO_X Traps*- Oak Ridge National Laboratory, Document Number: 2004-01-3023 – SAE technical papers.

[23] Joseph R. Theis, Justin A. Ura, John J. Li, Gopichandra G. Surnilla, John M. Roth, Christian T. Goralski. *NO_X release characteristics of Lean NO_X Traps during Rich Purges*- Ford Motor Co, Document Number: 2003-01-1159- SAE technical papers.

[24] Josh Pihl, James Parks, Charles Daw. *Product selectivity during regeneration of Lean NO_X Trap catalysts.* Oak Ridge National Laboratory, Document Number: 2006-01-3441- SAE technical papers.

[25] Brian West, Shean Huff, James Parks, Matt Swartz & Ron Graves. *In cylinder production of hydrogen during net lean diesel operation*- Oak Ridge National Lab, Document Number: 2006-01-0212- SAE technical papers.

[26] P.R.N. Childs, J. R. Greenwood, and C. A. Long. *Review of temperature measurement.* Review of scientific instruments volume 71, number 8 Aug 2000.

[27] Daniel Türler, Brent T. Griffith, and Dariush K. Arasteh. *Laboratory procedures for using infrared thermography to validate heat transfer models.* American Society for Testing and Materials, 1997.

[28] Carosena Meola and Giovanni M Carlomagno. *Recent advances in the use of infrared thermography*- Meas. Sci. Technology. 15 (2004) R27–R58.

[29] T. Astarita, G. Cardone, G.M. Carlomagno, C. Meola. *A survey on infrared thermography for convective heat transfer measurements.* Optics & Laser Technology- 32 (2000)- 593- 610.

[30] Manfred T. Reetz, Michael H. Becker. *Time-Resolved IR-Thermographic Detection and Screening of Enantio selectivity in catalytic Reactions*- Angewandte Chemie International Edition, Volume 37, Issue 19, Pages 2647 – 2650.

[31] J.Kellow, E.E.Wolf. *In situ IR thermography studies of reaction dynamics during CO oxidation on Rh-SiO_2 catalysts*- Catalysis Today, volume 9 (1991) 47-51.

[32] John C. Kellow and Eduardo E. Wolf. *Propagation of oscillations during Ethylene oxidation on a Rh/$Si0_2$ catalyst*. AIChE Journal Volume 37, Issue 12, Pages 1844 – 1848.

[33] Grigorios C. Koltsakis, Nikolaos Margaritis, Onoufrios Haralampous, Zissis C. Samara. *Development and experimental validation of a NO_X trap model for diesel exhaust*. Aristotle University Thessaloniki, Document Number: 2006-01-0471.

[34] Louise Olsson, Hans Persson, Erik Fridell, Magnus Skoglundh and Bengt Andersson. *A Kinetic Study of NO Oxidation and NO_X Storage on Pt/Al_2O_3 and Pt/BaO/Al_2O_3*. J. Phys. Chem. B 2001, 105, 6895-6906.

[35] Andrea Scotti, Isabella Nova, Enrico Tronconi, Lindia Castoldi, Luca Lietti and Pio Forzatti. *Kinetic study of lean NO_X storage over the Pt- Ba/ Al_2O_3 system.* Ind. Eng. Chem. Res 2004, 43, 4522-4534.

[36] Stephen Poulston, Raj R. Rajaram. *Regeneration of NO_X trap catalysts*. Catalysis Today 81 (2003) 603–610.

[37] Isabella Nova Lidia Castoldi, Luca Lietti, Enrico Tronconi and Pio Forzatti. *On the dynamic behavior of "NO_X-storage/reduction" Pt–Ba/Al_2O_3 catalyst.* Catalysis Today, Volume 75, Issue 1-4, July 2002, Pages 431-437.

[38] Wen Li, Francisco J. Gracia, Eduardo E. Wolf. *Selective combinatorial catalysis; challenges and opportunities: the preferential oxidation of carbon monoxide*. Catalysis Today 81 (2003) 437–447.

[39] Feng Qin and Eduardo E Wolf. *Infrared thermography studies of unsteady state processes during CO oxidation on supported catalysts*. Chemical Engineering Science. Vol. 49, No. 24A, pp. 4263-4267. 1994.

[40] A.Yu. Gladky, V.V. Ustugov, A.M. Sorokin, A.I. Nizovskii, V.N. Parmon, V.I. Bukhtiyarov. *Thermography study of propane oxidation to synthesis-gas over nickel.* Chemical Engineering Journal 107 (2005) 33–38.

[41] S. Hodjati, P. Bernhardt, C. Petit, V. Pitchon and A. Kiennemann. *Removal of NO_X: Part I. Sorption/desorption processes on barium aluminate.* Applied Catalysis B: Environmental Volume 19, Issue 3-4, 7 December 1998, Pages 209-219.

[42] Michalis Konsolakis and Ioannis V. Yentekakis. *The Reduction of NO by Propene over Ba-Promoted Pt/gamma-Al_2O_3 Catalysts*- Journal of Catalysis 198**,** 142–150 (2001).

[43] S. Balcon, C. Potvina, L. Salin, J.F. Temp`ere and G. Dj´ega-Mariadassou. *Influence of CO_2 on storage and release of NO_X on barium-containing catalyst*. Catalysis Letters 60 (1999) 39–43.

[44] Peter J. Schmitz & Ronald J. Baird- *NO and NO_2 Adsorption on Barium Oxide: Model Study of the Trapping Stage of NO_X Conversion via Lean NO_X Traps.* J. Phys. Chem. B 2002, 106, 4172-4180.

[45] Westerberg B, Fridell E. *A transient FTIR study of species formed during NO_X storage in the Pt/BaO/Al_2O_3 system*. Journal of Molecular Catalysis A; Chemical, Volume 165, Number 1, 8 January 2001, pp. 249-263(15).

[46] Rachel L. Muncrief, Pranav Khanna, Karen S. Kabin, Michael P. Harold. *Mechanastic and kinetic studies of NO_X storage and reduction on Pt/Ba/ Al_2O_3.* Catalysis Today 98 (2004) 393-402.

[47] Yougen Kong, Sam Crane, Palak patel and Bill Taylor. *NO_X trap regeneration with an on board hydrogen generation device*. Society of Automotive Engineers Technical Series 2004-01-0582 (2004).

[48] Diesel Net website "*www.dieselnet.com*" copy right © 1997 - 2007 Ecopoint Inc " Jan-2007".

[49] *"www.wikipedia.org"* Wikipedia®- trademark of the Wikimedia Foundation Inc- "Jan-2007".

[50] " *www.epa.gov*" *U*.S Environmental protection agency, website- "Jan-2007".

[51] " *www.arb.ca.gov*" California Air Resources Board Home, website- "Jan-2007".

[52] *"WHO air quality guidelines global update 2005"*- Report on a working group meeting, Bonn, Germany, 18-20 October 2005- "Jan-2007".

[53] "www.unep.org" United Nations Environment Program. GEO Year Book 2003 website- "June-07"

[54] "www.ec.gc.ca" The Green Lane™, Environment Canada's World Wide Web site- "Jan-2007"

[55] "www.omnitekcorp.com" Copyright 2003, Omnitek Engineering, Corp "Feb-2007"

[56] "www.autocatalyst-recycling.umicore.com "Umicore Precious metals refining website- "Feb2007"

.

Appendix A: Sample calculation

Heat generated: The amount of heat generated on the catalyst surface from the given temperature profiles across each position was calculated as follows.

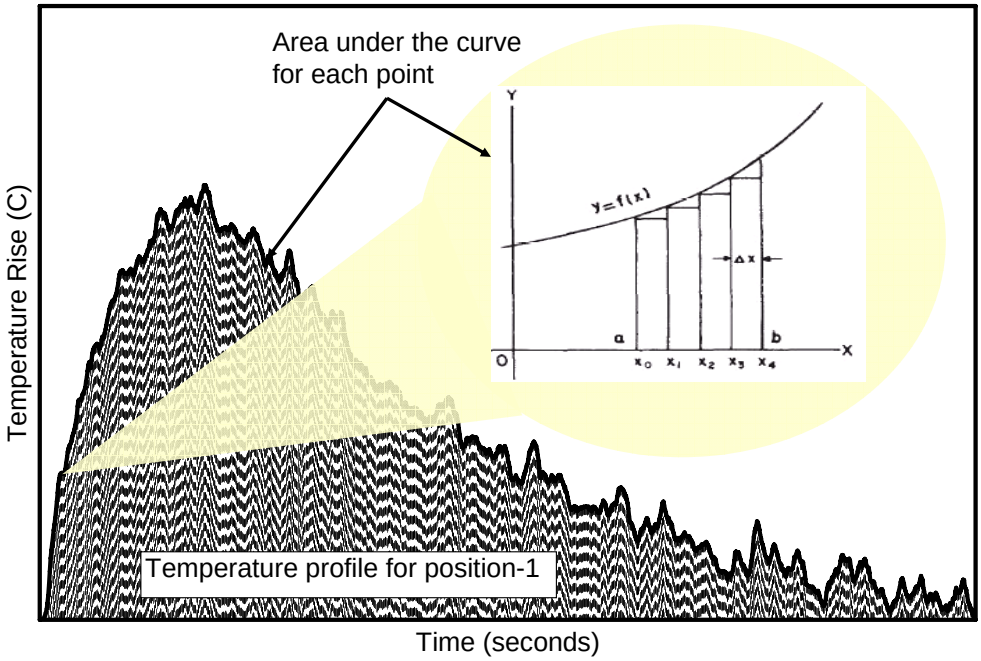

From graph

x= time in seconds and

y= f(x) which is the temperature rise so

Area under the curve for single rectangle = $\Delta A = (f(x).\Delta x)$

Total heat generated = Total area under the curve = $\lim_{n\to\infty} \sum_{k=1}^{n} (f(x)\ \Delta x)$

Where: $\sum$ represent the sum and n is the no of rectangles

The sum of all the rectangles will be approximately equal to the area under the curve, which is the amount of heat generated at individual point with respect to time. The units being (Delta temperature * delta time) = ^{o}C * seconds

Appendix B: Camera Images

a) Before induction of reductant (lean phase)

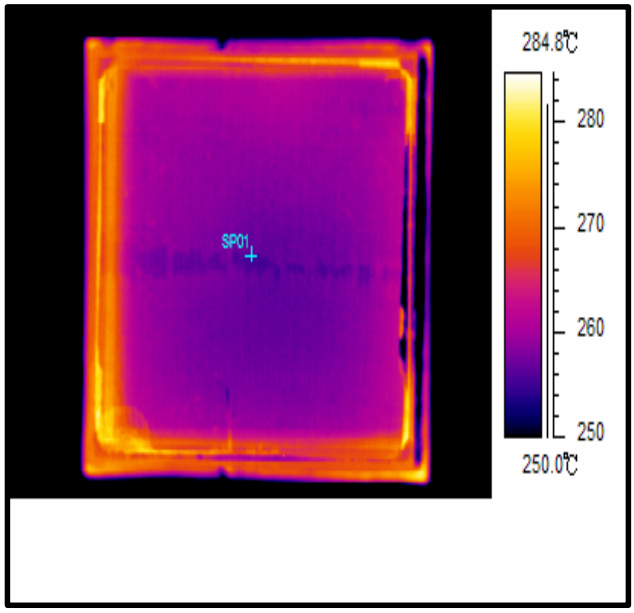

b) **After Induction of reductant (rich phase)**

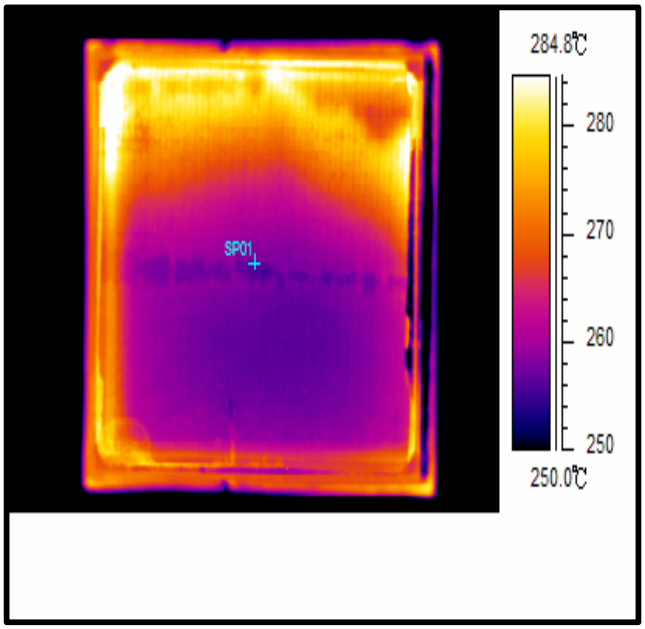

Appendix C: Temperature profiles for amount of NO_X trap

NO- 300°C

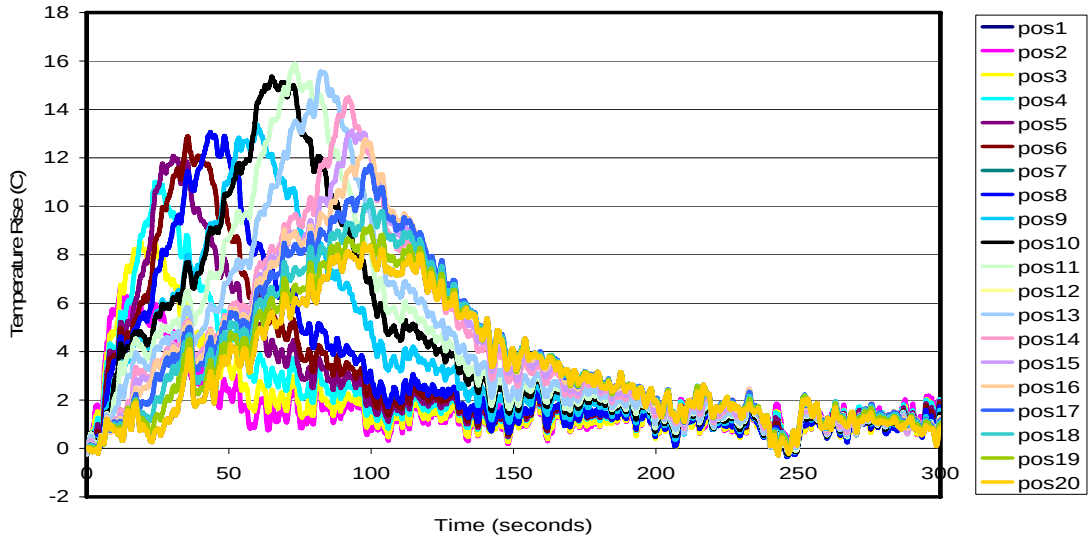

NO- 400°C

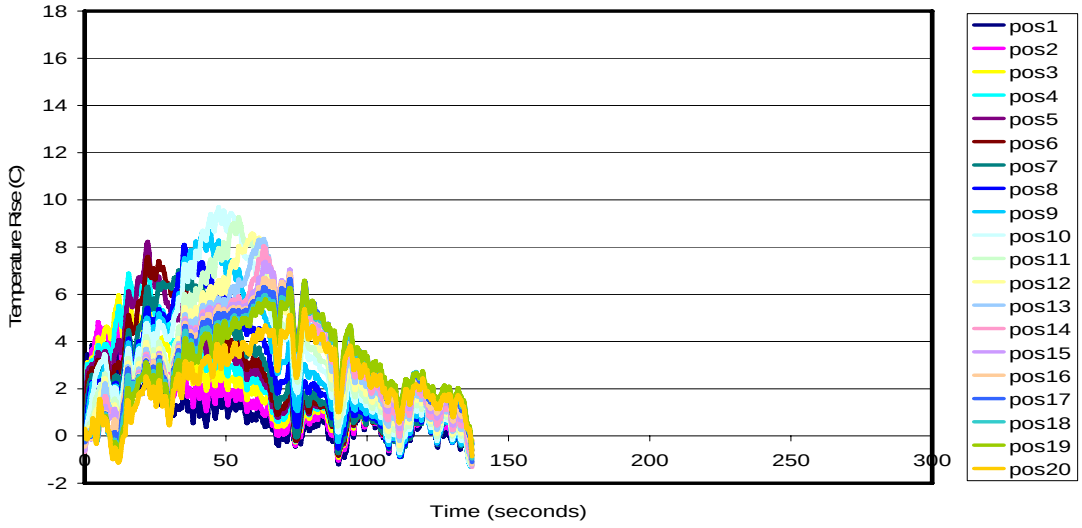

NO_2- 300°C

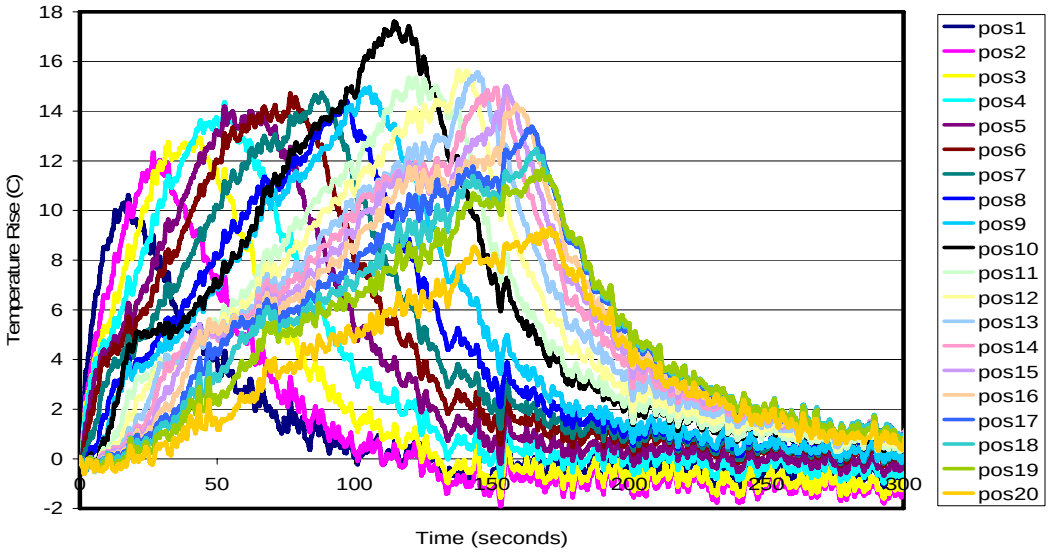

NO_2- 400°C